Experimental investigation of the electromagnetic sizes of the pion and kaon in πe and Ke elastic-scattering experiments

A. S. Vodop'yanov and É. N. Tsyganov

Joint Institute for Nuclear Research, Dubna

Fiz. Elem. Chastits At. Yadra **15**, 5–52 (January–February 1984)

Experimental investigations of the electromagnetic sizes of pions and kaons in πe and Ke elastic-scattering experiments are reviewed. The methods and results of experiments at 50, 100, and 250 GeV are considered in detail.

INTRODUCTION

Study of the structure of matter by means of the well-understood laws of electrodynamics has played an extremely important part in elementary-particle physics. The concept of an extended structure of elementary particles was formulated on the basis of experiments measuring the deviation of the differential cross section of electron scattering by hydrogen nuclei from the cross section for a point object. The first ep scattering experiments were made by Hofstadter in 1955.[1] In these experiments, 500–1000-MeV electrons bombarded target protons. The angular distribution of the scattered electrons did not correspond to what was expected for a point proton. The results of the experiments stimulated great interest among theoreticians and experimentalists in this problem in the following years. To explain the electromagnetic structure of the nucleon, Nambu[2] postulated in 1957 the existence of a two-pion state (the ρ mesons) as a intermediary in the photon–nucleon coupling. Later Frazer and Fulco[3] developed these ideas and predicted the existence of other mesons in the form of two-and three-pion resonance states. After the discovery of the ρ, ω, and φ mesons, Sakurai[4] proposed the vector-dominance model, in which it is assumed that the mechanism of exchange of the vector mesons ρ, ω, and φ plays the dominant part in the interaction of hadrons with the electromagnetic field. Many electromagnetic processes can be treated in a unified manner in the model. However, it encounters difficulties in the description of the proton charge radius and does not predict the observed dependence of the nucleon form factor on the momentum transfer.

The Feynman diagram for elastic electron–hadron scattering is shown in Fig. 1a. The differential cross section for scattering of a particle with zero spin and charge Ze by a spinless nucleus with charge ze is described in the nonrelativistic case by the Rutherford formula[5]

$$\frac{d\sigma}{d\Omega}=\frac{4m^2(zZe^2)^2}{q^4},$$

where $\mathbf{q}=\mathbf{p}-\mathbf{p}'$ is the momentum transfer. The scattering of an electron, which has spin $\frac{1}{2}$ and charge $z=1$, by a spinless target particle was considered by Mott.[6] For the effective scattering cross section for the case of single-photon exchange he obtained

$$\left(\frac{d\sigma}{d\Omega}\right)_{\mathrm{M}}=4(Ze^2)^2\frac{E^2}{(qc)^4}\left(1-\beta^2\sin^2\frac{\theta}{2}\right).$$

Here, E is the energy of the electron, and $v=\beta c$ is its velocity. In the nonrelativistic limit $\beta\to 0$, Mott's expression goes over into Rutherford's. Investigating the effects of the charge distribution on the scattering of fast electrons by nuclei, Guth[7] and Rose[8] showed that the scattering cross section in the case of a spherically symmetric charge distribution $\rho(\mathbf{r})$ in the nucleus differs from the Mott cross section by a factor $|F(\mathbf{q}^2)|^2$:

$$\frac{d\sigma}{d\Omega}=\left(\frac{d\sigma}{d\Omega}\right)_{\mathrm{M}}|F(\mathbf{q}^2)|^2,$$

this factor being related to the charge distribution $\rho(\mathbf{r})$ by the

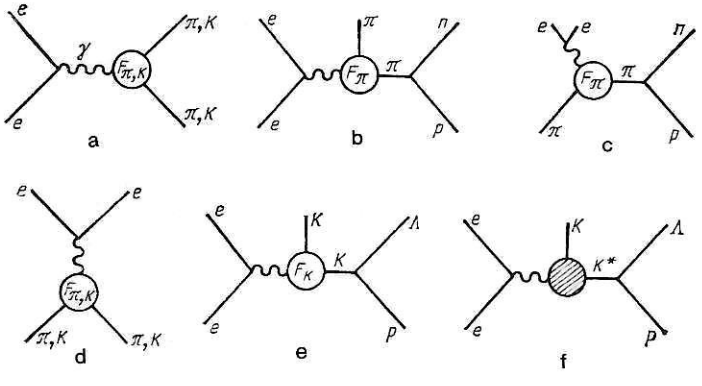

FIG. 1. Feynman diagrams for: a) elastic scattering of an electron by a hadron; b) pion electroproduction; c) inverse pion electroproduction; d) annihilation of an e^+e^- pair into hadrons; e) kaon electroproduction; f) kaon electroproduction with exchange of a K^* pole.

 0090-4759/84/010001-24$04.40

TABLE I. Form factors for some one-parameter charge distributions.

	Charge distribution	Form factor
Point	$\rho(r)=\delta(r-r')$	$F(q^2)=1$
Exponential	$\rho(r)=\frac{a^3}{8\pi}e^{-ar}$	$F(q^2)=\left(\frac{1}{1+q^2/a^2}\right)^2$
Yukawa type	$\rho(r)=\frac{a^2}{4\pi r}e^{-ar}$	$F(q^2)=\frac{1}{1+q^2/a^2}$
Gaussian	$\rho(r)=\left(\frac{a^2}{2\pi}\right)^{3/2}e^{-\frac{a^2r^2}{2}}$	$F(q^2)=e^{-q^2/2a^2}$

expression

$$F(\mathbf{q}^2)=\int \rho(\mathbf{r})\, e^{i\mathbf{q}\cdot\mathbf{r}} d^3r,$$

where it is assumed that

$$\int \rho(\mathbf{r})\, d^3r=1.$$

For $qr\ll 1$ and under the assumption that $F(\mathbf{q}^2)$ is a smoothly varying function, there exists a connection between the form factor and the mean-square charge radius $\langle r^2\rangle$ of the nucleus[9]:

$$F(\mathbf{q}^2)=1-\frac{1}{6}\mathbf{q}^2\langle r^2\rangle+\ldots \qquad (1)$$

Here

$$\langle r^2\rangle=\int \rho(\mathbf{r})\, r^2 d^3r.$$

It can be seen from the expression (1) that the form factor depends only on the square of the momentum transfer and not on the energy of the incident particle. Table I gives examples of the form factors for different charge distributions.[10]

From the expression (1), we find

$$\langle r^2\rangle=-6\frac{dF(q^2)}{dq^2}\Big|_{q^2=0}.$$

Thus, by studying electron–hadron (or hadron–electron) scattering, we can obtain information about the spatial distribution of charge in the hadron. Finally, we note that the analysis of elastic electron scattering in terms of electromagnetic form factors is based on two assumptions.

1) the validity of quantum electrodynamics for leptons;

2) the validity of the single-photon approximation.

The validity of quantum electrodynamics has been verified in many experiments. The single-photon exchange approximation is based on the small value $\alpha\approx 1/137$ of the fine-structure constant. This assumption is also well confirmed by experimental data.[11]

The interpretation of scattering processes based on these two assumptions shows that to study the electromagnetic interaction of elementary particles one can use perturbation theory and make a restriction to the lowest nonvanishing approximation. In the lowest approxiation in e, the matrix element of the process (Fig. 1a) contains a scalar function $F_1(t)$. The process of electron–positron annihilation into two pions (Fig. 1d) also contains a function $F_2(s)$, which depends on the square of the total c.m.s. energy of the particles. These functions are related. The intimate connection between the matrix elements of crossed processes is well known in quantum electrodynamics. There exists a function $F(\omega)$, analytic in the complex ω plane with a cut $\omega\geqslant 4\mu^2$ (μ is the pion mass), that is equal to $F_1(t)$ for $\omega=t\leqslant 0$ and tends to $F_2(s)$ as $\omega\to s$ from the upper plane. In other words, each of the functions $F_1(t)$ and $F_2(t)$ is the analytic continuation of the other. The function $F(\omega)$ is called the pion form factor. Form factors for the other particles are introduced similarly.

The electromagnetic form factors carry information about the strong-interaction processes in the hadron that determine the electromagnetic structure of the particles. Moreover, the quantitative description of strong interaction is made in the framework of a functional dependence on the single variable q^2. This circumstance is responsible for the fact that modern methods of the theoretical physics of elementary particles (for example, quantum chromodynamics) are widely used to describe form factors.

1. BRIEF REVIEW OF INVESTIGATIONS OF THE ELECTROMAGNETIC FORM FACTORS OF THE PION AND KAON

The Pion Radius

Since the charged pions and kaons do not have spin, they can be characterized by a single electromagnetic form factor. Accurate measurement of their form factors is extremely important for the study of various theoretical models.

A large number of experiments have been made to determine the electromagnetic pion radius (Table II). When positive and negative pions are scattered by helium nuclei,[12–14] the difference between the scattering cross sections is proportional to the product of the form factors of the pion and the helium nucleus. Knowing the charge radius of the helium nucleus and its nuclear amplitude, we can obtain the pion form factor. However, the procedure for determining the pion form factor is sensitive to the assumptions made about the nuclear amplitude and the influence of the Coulomb interaction. For example, Christensen,[15] who used a relativistic model, obtained $r_\pi\sim 1$ F from $\pi\alpha$ scattering data; Nichitiu and Shcherbakov,[16] who used other phase shifts, obtained $r_\pi=(0.80\pm 0.40)$ F; Auerbach *et al.*[17] give $r_\pi<2.0F$ in the optical-theorem approxiation; and Aleksan-

TABLE II. Experimental data for the charge radius of the π^- meson.

Experimental technique	$\langle r_\pi^2 \rangle^{1/2}$, F	Reference
	$\pi\alpha$ scattering	
Counters	1.8 ± 0.8	Ref. 12
Helium bubble chamber	<0.9	Ref. 13
Counters	2.96 ± 0.43	Ref. 14
	Pion electroproduction	
Counters	0.80 ± 0.10	Ref. 19
Counters	0.86 ± 0.14	Ref. 20
Counters, wire chambers	0.704 ± 0.025	Ref. 21
Counters, wire chambers	0.711 ± 0.018	Ref. 22
Counters	$0.740 \pm \begin{matrix} 0.11 \\ 0.13 \end{matrix}$	Ref. 23
	Inverse electroproduction	
Counters, spark chambers	<1.9	Ref. 28
Counters, spark chambers	0.60 ± 0.11	Ref. 29
Counters, spark chambers	0.62 ± 0.12	Ref. 30
	Colliding electron–positron beams	
Counters, proportional chambers	0.678 ± 0.011	Ref. 37
Counters	0.605 ± 0.039	Ref. 38
	Elastic πe scattering	
Propane bubble chamber	<6.6	Ref. 44
Hydrogen bubble chamber	<4.5	Ref. 45
Counters, spark chambers	<3.3	Ref. 47
Counters, spark chambers	0.78 ± 0.10	Ref. 48
Counters, spark chambers, and proportional chambers	0.56 ± 0.04	Ref. 49
Counters, drift chambers, and proportional chambers	0.66 ± 0.03	Ref. 50

drov *et al.*[18] obtained $r_\pi = (0.83 \pm 0.17)$ F. It is evident that this method cannot pretend to a particularly accurate determination of the electromagnetic pion radius. In pion electroproduction experiments (Fig. 1b),[19–23] the reaction

$$e^- + p \to e^- + \pi^+ + n$$

was studied.

In 1959, Frazer[24] showed that from experiments of this kind, using a Chew–Low-type extrapolation of the differential cross sections to $q^2 = \mu^2$ (μ is the pion mass), one can obtain a model-free determination of the pion form factor. Since then, the accuracy of the experiments on this reaction has improved by between one and two orders, but it is still far from sufficient for making any definite extrapolation to the pion pole. Therefore, in pion-electroproduction experiments information about the pion form factor is usually extracted on the basis of the Born model and the calculation of corrections to it by means of dispersion relations for fixed q^2 (Berends's methods[25]). In the theoretical interpretation of the experimental data, it is assumed that the imaginary part of the amplitude for production of a single pion is small and completely determined by the isobar Δ (1236). The isovector part of the cross section of the investigated process is calculated and its experimental value found by comparing the data obtained using hydrogen and deuterium targets, it being assumed that the nucleons in the deuterium nucleus are free. In this way, the rms pion radius 0.704 ± 0.025 F was obtained in Ref. 21. The systematic error in the experimental data on the differential cross sections is estimated at 5–6%. Although the authors show that the employed model gives a reasonable description of different aspects of the experimental data when the produced pions are emitted at small angles relative to the direction of the virtual photon, the theoretical uncertainty in the interpretation of the data remains very great. The model-dependent nature of these measurements poses many theoretical questions. For example, in Ref. 26 it is noted that the subtraction constant used in Berends's dispersion calculations[25] contains an unknown function of t and k^2 (k^2 is the square of the "mass" of the virtual photon), which introduces an ambiguity into the definition of the pion form factor. In Ref. 27, it is pointed out that in theoretical dispersion calculations it is also necessary to take into account the contribution of the axial-vector form factor.

Drell and Zachariasen[9] pointed out the possibility of determining the pion form factor by means of inverse pion electroproduction, in which a virtual photon produces an electron–positron pair (Fig. 1c).

This reaction[28–30]

$$\pi^- + p \to e^- + e^+ + n$$

makes it possible to study the form factor in the region $-4m_\pi^2 < q^2 < 0$ $(GeV/c)^2$, which is kinematically inaccessible for other types of experiments. In the single-photon approximation, this process can be described in accordance with the T invariance by the same amplitude as pion electroproduction, only the ranges of variation of k^2 being different. However, to determine the form factor, model-dependent dispersion calculations are needed here too. In Ref. 30, the experimental data were analyzed in the framework of the model of Ref. 31, which takes into account only the contribution of the magnetic-dipole transition amplitude M_{1+}. The model parameters used are the Dirac and Pauli isovector and isoscalar nucleon form factors $F_1^v, F_2^v, F_1^s, F_2^s$, the pion form factor F_π, and the form factor G_M^*, which occurs in the amplitude M_{1+}. In the analysis, the form factors F_1^v and F_π were taken to be real and equal:

$$F_1^v\ (k^2) = F_\pi\ (k^2).$$

The form factors were determined with an error of about 6%. However, if the form factors F_1^v and F_π are assumed to be independent, the resulting values have an error of about 80%.

In a number of theoretical studies[32–33] it has been shown that the difference $\Delta\ (k^2) = F_1^v(k^2) - F_\pi(k^2)$ can be calculated with fairly good accuracy. In an analysis of experimental data in Ref. 29, the form factors F_1^v and F_π were calcuated by means of the dispersion model of Ref. 31 using the theoretical values of their difference. The electromagnetic pion radius was found to be

$$\langle r_\pi^2\rangle^{1/2} = (0.60 \pm 0.11)\ \text{F}\ .$$

Thus, these indirect methods of determining F_π involve theoretical uncertainties associated with the models employed.

The pion form factor can also be measured in the timelike region of momentum transfers[34–38] in colliding-beam experiments:

$$e^+ + e^- \to \pi^+ + \pi^-.$$

In this case, the square of the momentum transfer is $t = s = (2E)^2$, and the total cross section of the process (Fig. 1d) can be written in the form[39]

$$\sigma = \frac{\pi\alpha^2}{12E^2}\beta_\pi^3 |F_\pi|^2,$$

where β_π is the velocity of the pion, and E is the energy of the beam. In these experiments, it is usual to detect simultaneously e^+e^- interaction events with final state e^+e^-, $\mu^+\mu^-$, *or* $\pi^+\pi^-$. In this case, the square of the modulus of the pion form factor can be expressed in terms of the experimentally determined event numbers $N(\pi\pi)$ *and* $N(ee + \mu\mu)$ as follows[38]:

$$|F_\pi|^2 = \frac{C1\sigma_{ee} + C2\sigma_{\mu\mu}}{C3\sigma_{\pi\pi}} \frac{N(\pi\pi)}{N(ee+\mu\mu)},$$

where $\sigma_{ee}, \sigma_{\mu\mu}, \sigma_{\pi\pi}$ are the electromagnetic cross sections of the processes $e^+e^- \to e^+e^-, \mu^+\mu^-, \pi^+\pi^-$, and $C1, C2, C3$ are correction coefficients. It should be noted that in these experiments the form factor can be measured only in the t region above the threshold for production of a $\pi^+\pi^-$ pair $(t > 4m_\pi^2)$.

In the experiments of Refs. 34–36, F_π was measured in the neighborhood of the ρ-meson peak. The experimental data can be well described by the Gounaris–Sakurai expression[40] obtained in the vector-dominance model. However, to extract information about r_π it is necessary to know the behavior of the form factor in the region of t below the ρ peak near the pair-production threshold. In Ref. 37, the experimental data obtained with the colliding beams at Orsay were analyzed in the framework of the vector-dominance model with allowance for the contribution of the inelastic $\omega\pi$ channel.[41,42] The result was $\langle r_\pi^2\rangle^{1/2} = 0.678 \pm 0.011$ F. This is the currently most accurate result. In an experiment made at Novosibirsk using the storage facility VÉPP-2M,[38] the pion form factor was measured near the $e^+e^- \to \pi^+\pi^-$ threshold using a time-of-flight detector. The values obtained for F_π agree well with the predictions of the vector-dominance model. Approximation of the experimental data by the expression

$$F_\pi\ (s) = F_\pi^{GS}\ (s)\ G\ (s),$$

where $F_\pi^{GS}(s)$ is the pion form factor in the Gounaris–Sakurai model, and $G(s)$ is a smooth analytic function taking into account the contribution of distant inelastic channels, gives $\langle r_\pi^2\rangle^{1/2} = 0.605 \pm 0.039$ F. This value differs by two standard deviations from the results of the Orsay experiment.

Study of elastic πe scattering

$$\pi^- + e^- \to \pi^- + e^-$$

is the only model-independent way of measuring the pion charge radius. The theoretical differential cross section of the process for a point pion was obtained in Refs. 52 and 53:

$$\frac{d\sigma}{dE} = 2\pi r_e^2 m_e \left(\frac{\gamma^2}{\gamma^2-1} - \frac{E}{E_{\max}} + \frac{m_e E}{2P_0^2c^2}\right)\frac{1}{E^2},$$

where E is the energy of the scattered electron in the laboratory system, $E_{\max}$ is the maximal energy transferred to the electron, P_0 is the momentum of the initial pion, γ is the Lorentz factor for the beam particles, r_e is the classical radius of the electron, and m_e is the electron rest mass. Bearing in mind that at giga-electron-volt energies

$$\gamma^2/(\gamma^2 - 1) \simeq 1, \quad m_e E/2P_0^2c^2 \simeq 0,$$

we can write the cross section in the form

$$\frac{d\sigma}{dE} = K\left[1 - \frac{E}{E_{\max}}\right]\frac{1}{E^2},$$

where $K = 2\pi R_e^2 m_e = 254.9$ MeV·mb.

Up to now, nine experiments[43–52] have been made in the energy range from 1 to 300 GeV. The first experiments,[43–48] which were made at energies below 50 GeV, could establish only an upper limit for the pion radius because of the smallness of the form-factor effect and the inadequate instrumental resolution. For measurement of the electromagnetic pion radius the reduced de Broglie wavelength of the electron, $\pi = \hbar c/E$, must be comparable with the Compton wavelength $\hbar/m_\pi c$ of the pion. Table III gives estimates of the sensitivity of the πe scattering experiments made in different laboratories to the pion size.

The first measurement of the pion charge radius was in a πe scattering experiment with the Serpukhov accelerator at 50 GeV.[48] Later experiments using the Fermilab accelerator at Batavia at 100 and 250 GeV made it possible to determine the pion radius with appreciably high accuracy.[49,50]

In the simplest vector-dominance model, the pion form factor is determined as

$$F_\pi(q^2) = \frac{1}{1 + q^2/m_\rho^2},$$

where m_ρ is the mass of the ρ meson. The pion charge radius in this model is

$$\langle r_\pi^2\rangle^{1/2} = 0.63\ \text{F}\ .$$

All the currently known theoretical predictions for the pion charge radius are given in Table IV. In various papers[32,54–57] bounds have been calculated for the pion radius on the basis of experimental data in the timelike region using dispersion relations and an assumption of relatively definite behavior of

TABLE III. Estimates of the sensitivity of πe scattering experiments made in different laboratories to the size of the π^- meson.

Laboratory	P_π, GeV/c	$q^{\text{cms}}_{\max}$, MeV/c	$1/q_{\max}$, F
Berkeley	1.12	8	24.5
Dubna	4	29.7	6.6
CERN	16	86.4	2.3
Brookhaven	20	102	2.0
Serpukhov	50	192	1.03
Fermilab	100	293	0.67
CERN	250	487	0.41
	300	536	0.37

the form factor at large q^2. In Ref. 57, the experimental data in the timelike region were parametrized with allowance for the four resonances $\rho(776)$, $\rho_A(1100)$, $\rho'(1250)$, and $\rho''(1540)$. Many authors have calculated[58–67] limiting values of the pion charge radius by analyzing experimental data in the complete range of momentum transfers.

Predictions for the radius of the charged pion were also made in the framework of an extended vector-dominance model in Ref. 68, on the basis of the Chou–Yang geometrical model of hadron scattering,[69] by means of the superpropagator method in a theory of chiral type,[70] and in a relativistic quark model.[71]

In Ref. 72, the experimental data on the pion form factor in the spacelike and timelike regions of momentum transfer $[-9.77 < q^2 < 9.61\ (\text{GeV}/c)^2]$ were approximated simultaneously by a method that reduces the dependence on the choice of the theoretical models. The result was $\langle r_\pi^2\rangle^{1/2} = 0.68 \pm 0.02$ F. When the experimental data on pion electroproduction of Ref. 23 are eliminated from the analysis, $\langle r_\pi^2\rangle^{1/2} = 0.66 \pm 0.02$ F.

The Radius of the K^- Meson

In the vector-dominance model, the electromagnetic form factor of the charged kaon is given by [73]

$$F_K(q^2) = \frac{1}{2}\left(1+\frac{q^2}{m_\rho^2}\right)^{-1} + \frac{1}{8}\left(1+\frac{q^2}{m_\omega^2}\right)^{-1} + \frac{3}{8}\left(1+\frac{q^2}{m_\varphi^2}\right)^{-1}.$$

In accordance with this, the kaon charge radius is

$$\langle r_K^2\rangle^{1/2} = 0{,}58 \text{ F}.$$

In this model, the three vector mesons ρ, ω, and φ contribute to the kaon form factor. The extended vector-dominance model[68] requires the existence of at least three isovector and three isoscalar mesons. This model predicts $\langle r_K^2\rangle^{1/2} = 0.62$ F.

In Table V, we give the theoretical predictions for the kaon charge radius calculated on the basis of different models. In Ref. 74, the contribution of the isovector part of the kaon form factor is determined by means of dispersion relations, and the contribution of the isoscalar part is found using the vecto-dominance model. In Ref. 69, the K^- charge radius is estimated on the basis of the geometrical model of hadrons scattering. Volkov, Matafonov, and Pervushin[76] made predictions for r_{K^-} in quantum chiral theory. Volkonskiĭ[77] calculated the kaon radius by means of the parton model. Gerasimov[75] and Tarrach,[71] who used the relativistic quark model, obtained a limiting value for the kaon radius.

The kaon, like the pion, is a spinless particle and has a relatively small mass. Like the pion, it cannot be used as a target particle in electron elastic-scattering experiments because of its instability. Therefore, experiments to study kaon structure depend on the possiblity of obtaining beams of high-energy kaons to be used for elastic scattering on atomic electrons. Attempts to use the electroproduction method to measure the kaon electromagnetic form factor encounter serious difficulties because of the large kaon mass, and also because of the impossibility of distinguishing the contribution to the reaction $e^- + p \to e^- + K^+ + \Lambda^0$ of the reaction with exchange of a K-meson pole (Fig. 1e) from the contribu-

TABLE IV. Theoretical predictions for the charge radius of the π^- meson.

$\langle r_\pi^2\rangle^{1/2}$, F	Reference	$\langle r_\pi^2\rangle^{1/2}$, F	Reference
0.58 – 0.69	Ref. 54	0.63	Ref. 62
$0.69^{+0.01}_{-0.02}$	Ref. 55	0.7	Ref. 63
		0.71 ± 0.01	Ref. 64
0.24 – 0.78	Ref. 56	0.68 ± 0.01	Ref. 65
0.66 – 0.69	Ref. 32	0.695	Ref. 66
0.69	Ref. 57	0.70 ± 0.15	Ref. 67
		0.65	Ref. 68
< 2.1	Ref. 58	0.61 ± 0.03	Ref. 69
< 0.67	Ref. 59	0.65	Ref. 70
0.49 – 0.74	Ref. 60	0.58 – 0.65	Ref. 71
0.68 ± 0.06	Ref. 61	0.68 ± 0.02	Ref. 72

TABLE V. Theoretical predictions for the charge radius of the K meson.

$\langle r_K^2\rangle^{1/2}$, F	Reference	$\langle r_K^2\rangle^{1/2}$, F	Reference
0.58	Ref. 73	0.52 – 0.77	Ref. 71
0.62	Ref. 68	0.61	Ref. 76
0.620 ± 0.037	Ref. 74	0.52	Ref. 77
0.54 ± 0.13	Ref. 69	0.56	Ref. 78
0.53 – 0.63	Ref. 75		

tion of the diagram with exchange of a K^* pole (Fig. 1f). Although kaon electroproduction experiments have been made,[79] results on the kaon form factor have not been published.

Some experiments to determine the kaon electromagnetic form factor in the timelike region of momentum transfers have been made using colliding electron–positron beams.[80–91] A reaction of the type

$$e^+ + e^- \to K^+ + K^-$$

was studied.

Figure 2 shows the currently known data on the kaon form factor in the timelike region of momentum transfers. The experimental data are compared with the prediction of the vector-dominance model taking into account the contributions of the ρ, ω, and φ mesons.[90] It can be seen that the data in the region of excitation energies higher than 1.1 GeV lie above the theoretical curve. This is evidently due to the contribution of the inelastic channels.[92,93] There are as yet insufficient data in the timelike region for a model-free extrapolation of the kaon form factor to $q^2 = 0$ and calculation of its charge radius with reasonable accuracy. In Ref. 78, the experimental data on the kaon form factor in the timelike region were analyzed in the framework of a resonance model that takes into account the contributions of the ρ mesons and the heavier vector mesons. The rms K^- radius obtained there is 0.56 F.

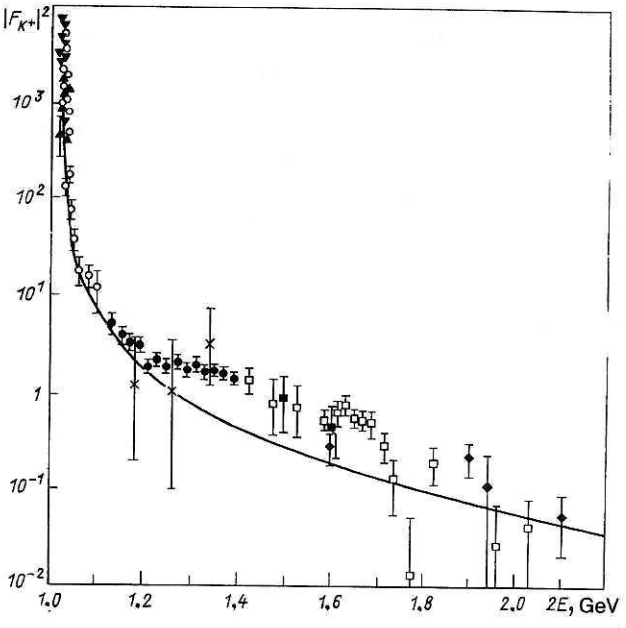

FIG. 2. Experimental data on the kaon form factor in the timelike region of momentum transfers: black triangles, Orsay (1970); inverted black triangles, Novosibirsk (1971); crosses, Novosibirsk (1972); black diamonds, Frascati (1973–1975); open circles, Novosibirsk (1976); black squares, Frascati (1977–1980); open squares, Orsay (1979–1981); black circles, Novosibirsk (1979).

The first (and as yet the only) experiment in which the electromagnetic radius of the K^- meson has been measured is a Ke elastic-scattering experiment made at Fermilab at energy 250 GeV.[94] The rms kaon radius was found to be

$$\langle r_K^2\rangle^{1/2} = (0.56 \pm 0.05)\ \text{F}.$$

Because of the distinguished status of Ke and πe scattering experiments for the problem of determining the electromagnetic form factors of the kaon and pion, which permit an almost model-free interpretation of their results, we shall consider these experiments in more detail.

2. ELASTIC Πe AND Ke SCATTERING EXPERIMENTS

In the experiments described in detail below, elastic scattering of π^- mesons with momentum from 1 to 300 GeV/c and K^- mesons with momentum 250 GeV/c by atomic electrons was studied.

The kinematics of the πe scattering process can be described by the 4-vectors P_e, P_e', P_π, P_π' (Fig. 3).The 4-momentum transfer depends only on the energy of the scattered electron:

$$-q^2 = (P_e - P_e')^2 = (P_\pi - P_\pi')^2$$
$$= 2m_e\,(m_e - E_e) \simeq -2m_e E_e,$$

where m_e is the electron mass, and E_e is the electron energy in the laboratory system (i.e., in the system in which the initial electron is at rest). The maximal energy that the recoil electron can acquire in the laboratory system is

$$E_{\max} = \frac{P_0}{1 + m_\pi^2/(2m_e P_0)},$$

where P_0 is the momentum of the initial beam.

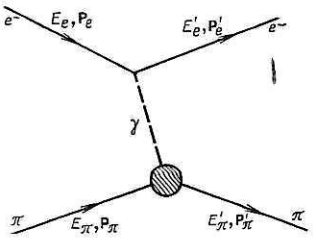

FIG. 3. Feynman diagram for elastic πe scattering.

TABLE VI. Maximal effect of the nonpointlike nature of the pion and kaon for different energies of the initial beam.

Particle	Energy, GeV				
	20	50	100	250	300
π	1.03	1.14	1.31	1.94	2.19
K	—	1.03	1.12	1.40	1.53

The sensitivity of such an experiment to the charge structure of the particle can be estimated if one knows (or assumes) the form factors of the particles. Table VI gives the maximal effect of the difference of the pion and kaon from points for different energies of the initial beam. These estimates were obtained using the values of the form factors predicted by the vector-dominance model. It can be seen that for the pion the effect is comparatively large already at beam energy 50 GeV, whereas for the kaon the effect becomes appreciable only at 100 GeV and above.

Elastic πe Scattering Experiments in the Energy Range 1–20 GeV (Refs. 43–47)

Elastic πe scattering was studied for the first time using a 25-cm hydrogen bubble chamber at Berkeley in 1960.[43] The chamber was bombarded with a beam of 1.12-GeV/c pions. From 26 000 photographs, 212 events of πe scattering with electron beam energy from 32 to 62 MeV were selected. This made it possible to measure the total cross section of the process in the given range of electron energy:

$$\sigma = (1.37 \pm 0.17)\,\text{mb}.$$

The theoretical total cross section for a point pion in the same range is $\sigma_{\text{th}} = 1.17$ mb. Thus, in this experiment no difference of the pion from a point particle was noted.

An experiment in the High Energy Laboratory of the Joint Institute for Nuclear Research using a 24-liter propane bubble chamber[44] studied πe scattering with 4-GeV/c pions. About 50 000 frames were obtained, among which 573 events with electron energy $\geqslant$300 MeV satisfied the selection criteria. The total cross section was found to be

$$\sigma = (0.166 \pm 0.010)\,\text{mb},$$

which agrees well with the theoretical value $\sigma_{\text{th}} = 0.169$ mb. On the basis of the maximal value $q_{\max} = 29.7$ MeV/c of the momentum transfer, a limit was obtained for the pion radius:

$$r_\pi \leqslant 6.6 \text{ F}.$$

Two πe scattering experiments were made at CERN with 16-GeV/c pions. In the experiment of Ref. 45, the pion beam bombarded a 30-cm hydrogen bubble chamber. From 57 500 frames, 2702 events with electron energy from 30 to 7300 MeV were chosen. Various experimental corrections were taken into account in the determination of the differential cross section. The error in the measurement of the electron momentum varied from 4% at $P < 100$ MeV/c to 6% at $P \geqslant 500$ MeV/c, and the ionization and radiation losses varied from 3% at 30 MeV/c to 0.5% for $P > 60$ MeV/c.The beam contained 10% muons, 1% kaons, and 0.3% antiprotons. The correction to the hydrogen density was 2%. The total integrated cross section with events with $P > 30$ MeV/c was

$$\sigma = (8.69 \pm 0.19)\,\text{mb}.$$

The theoretical total cross section is $\sigma_{\text{th}} = 8.27$ mb. the square of the pion form factor was approximated by the method of maximal likelihood. From the distribution of the likelihood function it is concluded that the pion charge radius satisfies

$$r_\pi \leqslant 4.5 \text{ F}.$$

In the other experiment, made using the photoemulsion method[46] in 1979, the differential cross section of πe scattering at pion momentum 16.2 GeV/c was measured. The statistics included 189 events with electron energy from 100 to 3000 MeV. It was concluded that in the investigated region of momentum transfers the experimental cross section does not differ from the cross section for a point pion.

In an experiment made at Brookhaven[47] use was made of a magnetic spectrometer consisting of optical spark chambers, a liquid-hydrogen target, scintillation counters, and an analyzing magnet. The pion beam momentum was 20 GeV/c. In this experiment, the largest possible 4-momentum transfer was 0.01 (GeV/c)^2. An upper limit for the pion radius was obtained:

$$r_\pi < 3.3 \text{ F}.$$

Because of the difficulties encountered in the experiment and in the analysis of the data, it was not possible to reduce significantly the upper limit on the pion radius compared with the previous experiment.

Elastic πe Scattering at 50 GeV (Ref. 48)

The first elastic πe scattering experiment in which it proved possible to measure the pion rms radius was made using the largest Soviet accelerator at Serpukhov in 1970–1971. The arrangement of the experiment with this accelerator was proposed by a group of physicists at the Joint Institute for Nuclear Research and independently by physicists from the University of California at Los Angeles. The investigations were made by the combined efforts of these two groups.

In the preparation of the experiment, πe scattering at 50 GeV was simulated under the assumption that $r_\pi = 0.7$ F.[95] The differential cross section was approximated after the introduction of the assumed geometrical efficiency by the method of least squares (Fig. 4). The calculations showed that at a beam energy of 50 GeV one can attempt to measure the pion charge radius with an error of not more than 0.05–0.10 F.

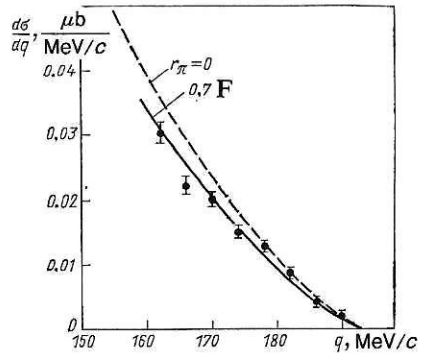

FIG. 4. Differential cross section of elastic πe scattering obtained by simulation with allowance for an assumed geometrical efficiency.[95]

A source of the hadron background in the experiment could be reactions of the type

$$\pi^- + p \to \pi^- + p + \pi^0;$$
$$\pi^- + p \to \pi^- + \pi^- + \Delta^{++}.$$

In Ref. 95, these reactions were analyzed, and it was shown that in a πe scattering experiment at 50 GeV the background level should not exceed 0.3% in the case of reliable identification of the secondary particles. Analysis of the experimental data subsequently showed that the strong-interaction background in this experiment was negligibly small.

The πe scattering reaction was studied in the region of momentum transfers $0.013 \leqslant q^2 \leqslant 0.036$ $(\mathrm{GeV}/c)^2$, or $13 \leqslant E_e \leqslant 36$ GeV, i.e., at the maximal attainable values of q^2 ($E_{\max} = 36$ GeV). The integrated cross section in this region is approximately 2 μb, which is appreciably less than the cross sections of typical hadronic processes. A feature of the studied reaction is the very small emission angles of the scattered electron and scattered pion (Fig. 5). The emission angle of the secondary pion does not exceed 3.6 mrad relative to the initial pion. The maximal angle between the secondary electron and secondary pion is less than 10 mrad in the entire range of q^2. For effective use of kinematic criteria, it was necessary to measure accurately the angles and momenta of the scattered particles and, in addition, have a reliable identification of the electron. We note that correct identification of the scattered electron was difficult at $E_e = E_\pi = 25$ GeV (Fig. 5). In this region of q^2, one cannot rely solely on the kinematics for the correct identification of an event.

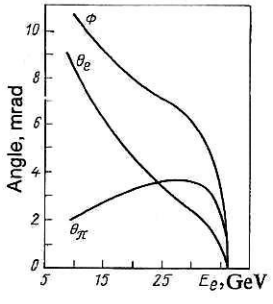

FIG. 5. Emission angles of the pion and the electron and the angle between the pair in elastic πe scattering at 50 GeV.

The experiment used a single-arm magnetic spectrometer, which detected both secondary particles (Fig. 6), and included magnetostriction spark and proportional chambers, combined into three blocks, a liquid-hydrogen target, an analyzing magnet, a muon detector, and a system of scintillation and Cherenkov counters used to trigger the facility. The spectrometer was operated on line to an HP 2116B computer.

Liquid hydrogen was chosen as the target because it has the highest electron density per unit mass (a minimum background from strong interactions) and gives the smallest radiative energy losses for the secondary electrons—the correction for absorption of the pions participating in the reaction is minimal for such a target. A high-precision 50-cm liqud-hydrogen target was prepared at the High Energy Laboratory at Dubna.[96] Stabilization of the pressure, flat windows, and a special screen shielding the working volume of the hydrogen from the bubbles produced by boiling make it possible to know the amount of hydrogen in the interaction region with an accuracy of about 0.05%.

To determine the trajectories of the primary particle and the secondary particles, 18 spark chambers with magnetostrictive readout and two proportional chambers were used. The information was read out from both the grounded and the high-voltage electrode of the spark chambers. The chambers were arranged in three blocks. The first was placed in front of the target, the second between the target and the magnet, and the third after the magnet. Two single-coordinate proportional chambers were placed between the spark chambers of the first block. At intensity 10^6 sec^{-1} of the initial beam, more than 50% of the events in the spark chambers were accompanied by background sparks from particles which passed through during the memory time of the chambers. Since the sensitivity time of proportional chambers is appreciably shorter (about 100 nsec) than for spark chambers, they were used to determine the coordinates in the first block of chambers that corresponded to a recorded track. Because it was necessary to distinguish two closely spaced tracks in the second block of the spectrometer, the information was read out from both ends of the magnetostriction tape in the spark chambers of the second block. This made it possible to separate sparks with a projection separation of 1.5 mm. In the chambers of the first and the third block of the spectrometer, sparks could be separated at a distance of 5 mm. For spatial comparison of the tracks of the particles, one chamber in the first block and two in each of the second and the third were rotated through 45°. The third block of spark chambers was used to measure the trajectory of the deflected particles. The efficiency of the spark chambers under the working conditions was about 95%. The random background sparks in the chambers reduced their efficiency, which imposed a restriction on the maximal intensity of the initial beam. To reduce multiple Coulomb scattering and energy loss by the electrons on radiation, polyethylene bags filled with helium were placed between the chambers and within the aperture of the magnet. The mean coordinate accuracy of the chamber, determined from the tracks, was found to be 0.35 mm for the high-voltage plane and 0.25 mm

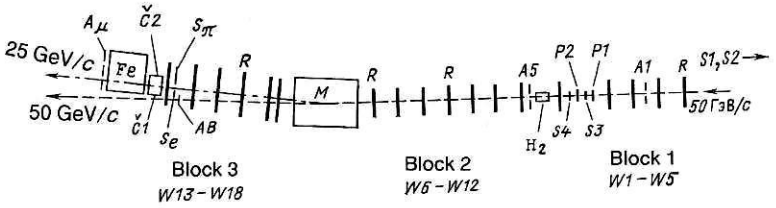

FIG. 6. Single-arm magnetic spectrometer used in the πe scattering experiment at 50 GeV. S 1–S 4 are beam scintillation counters; P 1 and P 2 are single-coordinate proportional chambers; W 1–W 18 are two-coordinate spark chambers; R are spark chambers rotated through 45°; H_2 is a liquid-hydrogen target; A 1, A 5, AB are anticoincidence counters; M is a magnet; S_e and S_π are the trigger scintillation counters. $\check{C}$ 1 and $\check{C}$ 2 are Cherenkov shower counters; Fe is an iron absorber; A_μ are scintillation counters for muon identification.

for the grounded plane. During the spill time of 1.2 sec, the apparatus could detect up to 120 events. In the experiment, the mean number of triggerings was 20 per accelerator cycle, the intensity of the incident beam being 2.5×10^5 particle/cycle.

The apparatus was triggered by means of scintillation counters and lead glass Cherenkov shower counters. The circuit of the fast electronics logic is shown in Fig. 7. The scintillation counters S 1–S 4, connected in coincidence and the anticoincidence counter A 1 with opening of diameter 8 cm, which was placed in front of the target and was used to cut off the wings of the beam, determined the flux of particles incident on the target. Behind the third block of spark chambers, scintillation counters S_e and S_π were placed to detect the two scattered particles. The accuracy of the determination of the differential cross section depended on the efficiency of these counters, and therefore each scintillator was scanned by two photomultipliers placed on opposite sides. For each event, the signals from both photomultipliers were recorded on magnetic tape, which make it possible to analyze the experimental data later and to show that the efficiency of both counters was very close to 100%. An anticoincidence counter A 5 with opening of diameter 10 cm was placed directly behind the target. In front of the counter there was a brass converter of two radiation lengths thickness, also with an opening. This counter was needed to suppress triggerings due to inelastic interactions in the target with angles between the particles greater than for the πe scattering. The anticoincidence counter AB was placed in the direction of the particles with momentum 50 GeV/c in the third block of the spectrometer. It served to suppress the random triggerings due to interaction of the beam particles with matter after the magnet.

In the experiment, the electrons were identified by means of two Cherenkov shower detectors with a lead glass radiator, which were placed behind the counters S_e and S_π. The energy resolution of these counters was $\sigma = 7\%\Delta E/E$ for electrons in the region of energies from 20 to 30 GeV. The apparatus was triggered in the case of coincidence of signals from the beam monitor, the counters S_e and S_π, one of the Cherenkov counters, and the absence of signals from the counters A 5 and AB.

The momenta of the scattered particles were measured with accuracy $\Delta P/P = \pm 0.4\%$ from the deflection of their trajectories in the magnet. Th HP 2116B computer and the software system make it possible to check the operation of not only the individual detectors but also the entire spectrometer during the collection of statistics.

About 2.5 million events were recorded, of which only about 40 000 satisfied the geometrical and kinematical crite-

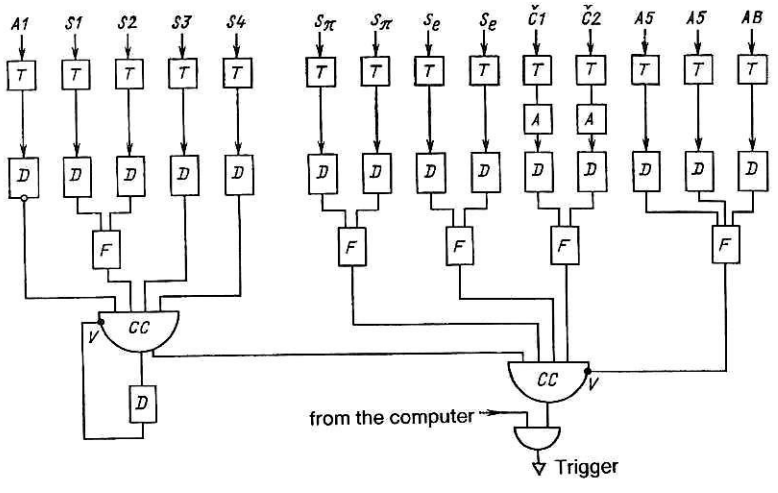

FIG. 7. System triggering circuit for πe scattering at 50 GeV. T is the delay block, D is a shaper discriminator, F is a multiplier, CC is the coincidence circuit, A is an attenuator, V is a veto, A 1, A 5, AB are anticoincidence counters, $\check{C}$ 1 and $\check{C}$ 2 are Cherenkov shower counters, and S 1–S 4 are beam scintillation counters.

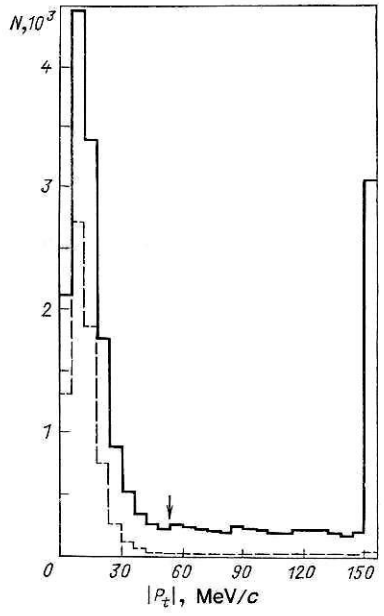

FIG. 8. Distribution of the number of πe events with respect to the transverse momentum. The continuous line gives the distribution before implementation of the selection criteria; the broken line, the distribution after their implementation except for the P_t criterion. The extreme right-hand column gives the sum of the events outside the histogram.

ria imposed on πe scattering events. The main kinematic criteria were formulated with allowance for the imbalance between the total and the transverse momentum, noncoplanarity, and the difference between the measured and calculated—on the basis of the particle momenta—emission angles of the secondary particles. Because of these criteria, the contribution of the background events was negligibly small. Figure 8 shows the distribution of the events with respect to the transverse momentum before and after implementation of all the adopted criteria except that for the transverse momentum. It can be seen that the contribution from inelastic events after implementation of the criteria is small. Figure 9 shows the distribution of the number of πe events with respect to the total momentum. The shape of this distribution corresponds to the spectrum of the beam particles with allowance for radiation loss in the matter of the spectrometer by the secondary electron. The cutoff with respect to the total momentum was set at ± 2 GeV/c.

The secondary electrons were identified using information from two Cherenkov shower counters and the kinematic quantity D^2 defined by

$$D^2 = \left(\frac{\theta_e^{\text{kin}} - \theta_e^{\text{exp}}}{\Delta\theta}\right)^2 + \left(\frac{\theta_\pi^{\text{kin}} - \theta_\pi^{\text{exp}}}{\Delta\theta}\right)^2.$$

In the case of electron identification solely by means of D^2 it was established that about 1% of the events from the region of small q^2 (electron energy less than 25 GeV) were identified as events from the region of large q^2 (electron energy greater than 25 GeV). This effect came about because of the emission of a photon during the πe scattering event. Since the elastic differential cross section in the region of large q^2 is small, the incorrect identification of the events distorted the cross section by about 10%. The additional information from the Cherenkov counters eliminated the ambiguity in the electron identification. On the other hand, if information from only the Cherenkov counters was used to identify the secondary particles, it was found that they were not identified in about 2% of the events, since the pulse heights in the counters were comparable. The use of D^2 ($D^2 < 10^{-6}$ rad^2) made it possible to identify such events correctly. Figure 10 shows the distribution of the Cherenkov-counter pulse height normalized by the electron energy.

An important aspect of the experiment was the experimental corrections to the data. Altogether, it was necessary to introduce about 20 corrections. The largest were those for the efficiency of event reconstruction, the geometrical efficiency, the radiation correction, the energy loss by the electrons on radiation in the material of the target and the spectrometer, and the absorption of pions in the material of the target and the spectrometer. The accuracy in the determination of the corrections appreciably influenced the accuracy in the determination of the pion radius.

The geometrical efficiency (Fig. 11) was calculated by means of the Monte Carlo method. The falloff of the efficiency in the region of small q^2 is due to the geometrical arrangement of the Cherenkov counters. Some data were obtained without requiring signals from the Cherenkov

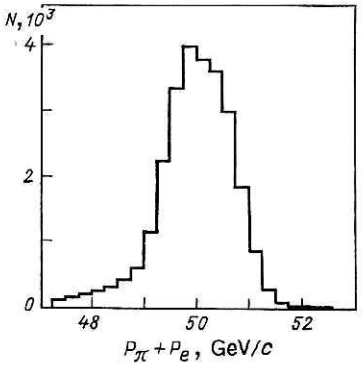

FIG. 9. Distribution of the number of πe events with respect to the total momentum.

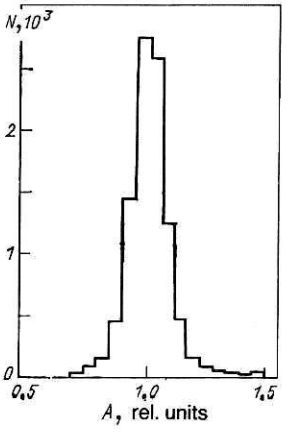

FIG. 10. Distribution of pulse heights (normalized by the electron energy) from the Cherenkov shower counters.

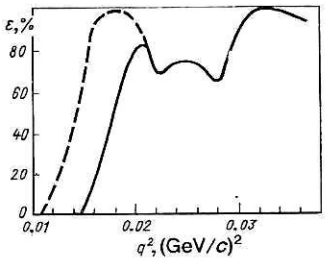

FIG. 11. Geometrical efficiency of the system in the πe scattering experiment at 50 GeV, calculated by the Monte Carlo method. The broken curve corresponds to a working session of the system without the requirement of a signal from the shower counters.

counters. In this case the falloff (broken curve) was determined by the edge of the scintillation counter S_π. The behavior of the curve in the region of q^2 around 0.025 $(\text{GeV}/c)^2$ is determined basically on the angular and momentum dispersion of the beam, its geometrical size, the presence of a vertical slit between the trigger counters S_e and S_π, the azimuthal dependence of the emission of the secondary particles, and the finite length of the target.

Two somewhat different approaches to the determination of the spectrometer efficiency and the reconstruction of elastic events were used. Both were based on Monte Carlo simulation of πe scattering with allowance for the actual experimental conditions. In the first approach, the main accent was on the use of background conditions in the spark chambers, which were extracted from the recorded πe scattering events, in order to avoid mathematical simulation of the processes of background loading of the chambers. In the second approach, in contrast, an attempt was made to simulate the background conditions under which the spark chambers operated in the experiment. Both approaches had their advantages and disadvantages and yielded somewhat different estimates of the spectrometer inefficiency. As a result, the data were analyzed using the mean value of the inefficiency (4%), and it was ascribed a systematic error equal to the difference between the values obtained by the two different methods (2%).

The radiation corrections reflect the effects associated with emission of a photon during the πe scattering event, and also energy loss by the electron on radiation in the target and the material of the spectrometer. The calculation of the radiation correction took into account the actual conditions of the experiment and the working criteria for event selection. The radiation correction is shown as a function of q^2 in Fig. 12. The calculations were made to terms of order α^3 in a program developed by Bardin, Micelmacher, and Shumeiko.[97] The main corrections are given in Table VII. The experimental differential cross section was calculated with allowance for all corrections. The square of the pion form factor was obtained by dividing the experimental cross section by the theoretically expected differential cross section for a point pion.

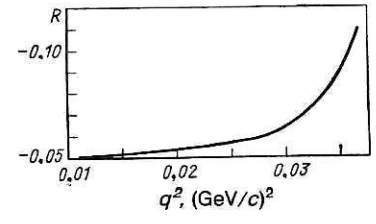

FIG. 12. Radiation correction for πe scattering at 50 GeV.

To detemine the pion charge radius, the form factors (Table VIII) were approximated by the so-called single-pole approximation,

$$|F_\pi|^2 = \frac{N}{\left(1 + \frac{1}{6}\langle r_\pi^2\rangle q^2\right)^2},$$

where N is a normalization coefficient that takes into account the systematic uncertainty in the experimental data. In this experiment it was equal to 2.8%. Since the systematic errors of the points were correlated, optimal allowance for the experimental errors was achieved by approximating the data using the complete error matrix M_{ij}, whose diagonal elements are the squares of the total errors. The correlation coefficients were calculated in accordance with the formula

$$C_{ij} = \frac{M_{ij}}{\sqrt{M_{ii}M_{jj}}}.$$

Completely uncorrelated errors give a unit matrix of correlation coefficients, while completely correlated errors give a matrix with all elements equal to 1. In the calculation of these correlation coefficients, the systematic errors had the maximal positive correlation between all pairs of points, since they represented the errors in the absolute normalization and influence all data points. An exception was made for the geometrical efficiency, in which only experimental points with small separation were assumed to be correlated. The value of χ^2 was calculated as follows:

$$\chi^2 = \sum_{ij} (T_i - E_i) M_{ij}^{-1} (T_j - E_j),$$

where E_i is the experimental value of the square of the form factor, and T_i is the theoretical value. This method of approximating the data takes into account the statistical errors and the proper correlation in the systematic errors in the most effective manner. As a result (Fig. 13), the following value was obtained for the pion radius:

$\langle r_\pi^2\rangle = (0.61 \pm 0.15)$ F^2 or $\langle r_\pi^2\rangle^{1/2} = (0.78 \pm 0.10)$ F.

Comparing this value with the prediction of the vector-dominance model,

$$\langle r_\pi^2\rangle / \langle r_{VDM}^2\rangle = (0.61 \pm 0.15)/0.40 = 1.54 \pm 0.38,$$

one cannot, however, yet draw a definite conclusion about the applicability of the model for the description of the pion form factor. This requires further experiments to determine the electromagnetic radius of the pion with greater accuracy.

In the πe scattering experiment at 50 GeV made with the Serpukhov accelerator the pion radius was measured for the first time in a model-independent way. The accuracy achieved in this experiment was about 30 times higher than the accuracy obtained in the previous πe scattering experiments. This investigation developed in detail all the methodological features of such experiments and was the prototype of all the later investigations made at high energies.

TABLE VII. Experimental corrections to the differential cross section in the πe scattering experiment at 50 GeV.

Effect	Correction, %	Error, %
Corrections not dependent on q^2		
Absorption of beam particles	2.7	0.6
Beam particles outside the kinematic momentum cuts: $48 < P < 52$ GeV/c	4.1	0.2
Random anticoincidences	3.2	0.7
Random coincidences of the beam monitor	1.0	0.2
Presence of K^- and $\bar{p}$ in the beam	1.2	0.1
Presence of μ^- in the beam in the interval $48 < P < 52$ GeV/c	0.5	0.1
Inefficiency of the Cherenkov shower counters	0.0	0.2
Inefficiency of scintillation counters	0.0	0.2
Anticoincidences from δ electrons from the target	1.6	0.2
Anticoincidences from hard photons emitted in the πe scattering event	0.3	0.2
Length of target	0.0	0.1
Mean values of the q^2-dependent corrections		
Emission in the target material and the spectrometer	19.0	0.9
Pion decay	1.0	0.1
Events from empty target	3.9	0.4
Background of inelastic hadron interactions	0.0	0.5
Absorption of pions in the spectrometer	1.8	0.3
Absorption of pions in the target	5.0	0.2
Loss of events due to cuts with respect to the Z position in the target	0.6	0.1
Admixture of μe scattering events	0.7	0.2
Energy calibration of the spectrometer	0.0	0.5

Elastic πe Scattering at 100 GeV (Ref. 49)

The electromagnetic form factor of the pion was investigated in elastic πe scattering at 100 GeV during 1975–1976 using the proton synchrotron at Fermilab (Batavia, USA). The experiment was made with participation of physicists from the Joint Institute for Nuclear Research. The core of this scientific collaboration was provided by the participants of the first JINR–USA collaboration at Serpukhov. The experiment was planned in the light of the experience of the earlier investigation.

The process of πe scattering was studied in the region of momentum transfers $0.03 \leqslant q^2 \leqslant 0.07$ (GeV/c)^2. The maximal angle between the scattered electrons did not exceed 8 mrad in the given region of q^2.

The experimental arrangement (Fig. 14) was based on spark and proportional chambers, a liquid-hydrogen target, two analyzing magnets, a muon detector, scintillation counters, a threshold Cherenkov counter, and lead glass shower counters. The experiment was run on line to an HP 2100 computer. It used 24 planes of proportional chambers,

TABLE VIII. Square of the pion form factor, measured in the πe scattering experiment at 50 GeV.

Number of point	q^2, (GeV/c)^2	$\lvert F_{\pi^-} \rvert^2$	Total error
1	0,0138	1,002	0,079
2	0,0149	0,991	0,073
3	0,0159	0,986	0,068
4	0,0169	0,983	0,075
5	0,0179	0,990	0,076
6	0,0190	0,924	0,046
7	0,0200	0,916	0,044
8	0,0210	0,946	0,044
9	0,0220	0,948	0,047
10	0,0231	0,918	0,047
11	0,0241	0,896	0,047
12	0,0251	0,905	0,048
13	0,0261	0,896	0,049
14	0,0272	0,894	0,053
15	0,0282	0,912	0,055
16	0,0292	0,847	0,050
17	0,0302	0,873	0,054
18	0,0312	0,910	0,054
19	0,0323	0,856	0,057
20	0,0333	0,742	0,066
21	0,0343	0,886	0,072
22	0,0353	0,849	0,093

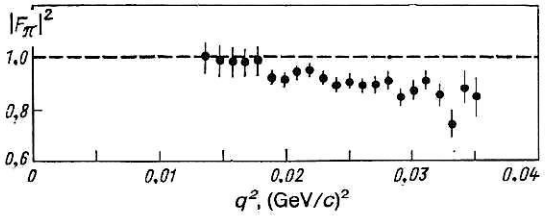

FIG. 13. Square of the pion form factor in the experiment at 50 GeV.

which were combined into blocks of four planes each, and six magnetostriction spark chambers measuring 1.5×0.5 m. The trajectories of the primary particle and the scattered particles after the target were measured by means of proportional chambers, and the trajectories after deflection in the magnets were measured by two-coordinate spark chambers. Following the earlier experiment at Serpukhov, the liquid-hydrogen target, which was 50 cm long and had diameter 10 cm, had a 1-m vacuum jacket at each end, which facilitated the reliable separation of target-event vertices from events due to the surrounding material. Two BM109 analyzing magnets were used in the spectrometer. The total integral of the field was 70 kG·m, which corresponded to deflection of a 100-GeV/c beam particle through 21 mrad. The field of each of the magnets was carefully measured and checked in the process of the experiment by the NMR method. The momentum resolution of the spectrometer for the scattered particles varied from 0.08% at 30 GeV/c to 0.3% at 100 GeV/c.

The trigger hodoscope consisted of the four scintillation counters *SE*, *SP*, *SU*, and *SD*. The last two covered the gap between the counters *SE* and *SP*, which improved the geometrical efficiency of the spectrometer. The electrons were identified by means of a system of ten lead glass shower counters. Eight blocks of glass measured $20\times20\times40$ cm, and two measured $12.5\times20\times40$ cm. The length of the blocks was 14 radiation units. The counters were arranged horizontally in two rows of five each. The rms error in the determination of the energy found for the elastic πe scattering events was $\pm$ 6%., Since the shower counters were used both to determine the electron energy and to form the trigger pulse, they were combined into groups of four each, and their signals were added. For each of the counters, a definite trigger threshold was set, corresponding to the minimal energy of an electron detected by the given counter. For each group of counters, a definite trigger threshold was also set. The resulting Cherenkov shower spectrometer signal was the logical sum of the signals from four groups of counters.

Muon–electron events in the experiment were identified by a muon detector, which consisted of an iron absorber of length 3.75 m and four scintillation counters.

The typical intensity of the primary beam in this experiment was $(2\text{–}4)\times10^5$ sec^{-1}. The identification of a "usable" beam particle required coincidence of signals from the scintillation counters B_0, B_1, B_2, the threshold Cherenkov counter $\check{C}_{TH}$, and the absence of a signal from the counter *AH* (anticoincidence counter with an opening of diameter 5 cm). In addition, the proportional chambers of the first block of the spectrometer were included in the logic of the beam monitor. First, a signal from three of the four planes in each module was required, and second, a double signal from any two planes in each of the modules forbade the shaping of a beam pulse. Besides these requirements, a condition of "zero beam intensity" was implemented by means of fast logic to reduce the number of background tracks in the proportional and spark chambers. For this, a signal from the counter B_0 was used to form a veto if some particle had passed through the system during the 1 msec before the working particle. To suppress events with two beam particles in one bunch (0.3 nsec), a signal from the counter B_2 set a veto if the pulse height in it exceeded by 1.5 times the pulse height for minimal ionization. Events for which some background particle passed through the system during the 1 μsec after the working particle were flagged. Only about one third of all the beam particles satisfied the above requirements.

The system trigger required the presence of signals from the beam monitor, the Cherenkov spectrometer, the trigger hodoscope, a two-particle signal from the proportional chambers of the second block, and the absence of a signal from the counter *A* 5 (anticoincidence counter with opening of diameter 10 cm). A two-particle signature was provided by the pulses from the proportional chambers *PWC* 5 and *PWC* 6. It was required that at least one horizontal and one vertical plane in each module record more than one particle.

In this experiment, about 10 000 elastic πe scattering events were selected by means of the geometrical and kinematical criteria. The kinematical selection of the elastic-scattering events[98] was made with allowance for the restrictions imposed by the energy–momentum conservation law.

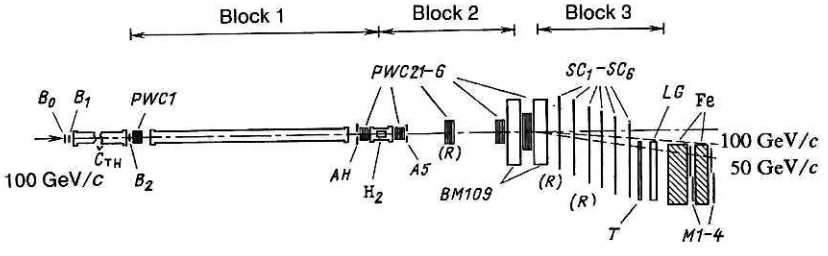

FIG. 14. Single-arm magnetic spectrometer for the πe scattering experiment at 100 GeV. *PWC* 1–6 are proportional chambers, SC_1–SC_6 are spark chambers, (*R*) are rotated chambers, B_0, B_1, B_2 are monitor scintillation counters, $\check{C}_{TH}$ is a threshold Cherenkov counter, H_2 is a liquid-hydrogen target, *AH* and A5 are anticoincidence scintillation counters, *BM* 109 are magnets, *T* is a trigger scintillation hodoscope, *LG* is the lead glass shower-counter array, Fe is an iron absorber, and *M* 1–4 are muon scintillation counters.

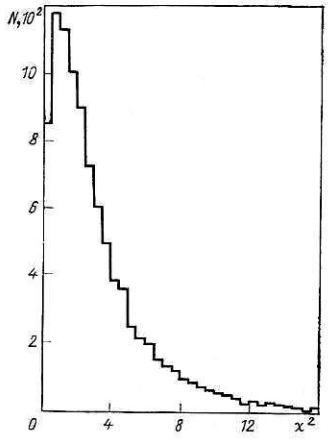

FIG. 15. The χ^2 distribution for πe scattering events in the experiment at 100 GeV.

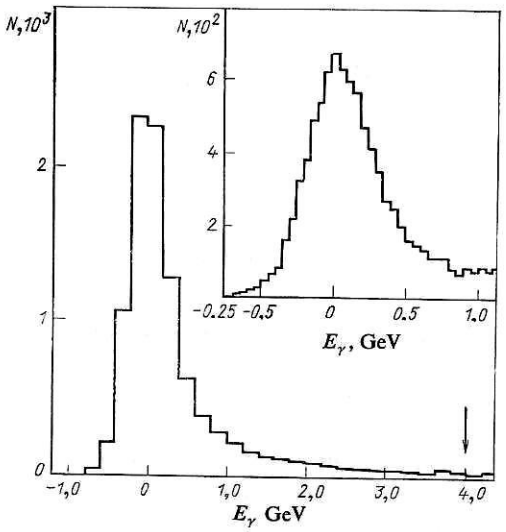

FIG. 16 Energy spectrum of emitted photons, obtained from kinematic analysis of the events. The arrow indicates the cut. In the top right corner the distribution near $E_\gamma = 0$ is shown.

In the analysis, it was assumed that an electron can emit a photon as it passes through the material of the spectrometer, it being then assumed that the photon is emitted in the direction of motion of the electron, and its energy was determined by an approximation procedure.

The χ^2 distribution was used to find the set of event parameters, including the energy of the emitted photon. As measured parameters, the directions and momenta of the secondary particles found in the experiment were used. The momentum of the primary beam was determined for each working session using the results of analysis of beam runs. To analyze an event, it was necessary to know the error matrix for the measured parameters. These errors were calculated using the characteristics of the experimental system.

The χ^2 distribution for the selected πe scattering events is shown in Fig. 15. The long tail of the distribution can be due to the hadron background as well as elastic scattering events. The latter can have a large χ^2 in the case of nuclear scattering of pions in the target or material of the spectrometer, pion decay in the spectrometer, internal emission of photons in the scattering event, a non-Gaussian shape of the distribution for multiple scattering of the particles, and possible errors in the geometrical reconstruction of the events. These effects lead to non-Gaussian errors in the measurements and are therefore difficult to take into account in the analysis of the events. Corresponding corrections were introduced for them in the calculation of the differential cross section. An event was rejected if $\chi^2 > 12$. The energy spectrum of the emitted photons obtained from the analysis of the events is shown in Fig. 16. It can be seen that the maximum of the distribution is situated around the origin. The width of the distribution is determined largely by the momentum spread of the primary beam. Events were rejected if the photon energy was greater than 4.0 GeV. Figure 17 shows the distribution of the Z coordinate of the reconstructed interaction vertex. The distribution is situated within the target. It can be seen that events from the target and events from other sources can be well separated. One further criterion for the selection of elastic events was the normalized (by the electron energy) Cherenkov-spectrometer pulse height (Fig. 18). An event was rejected if the pulse height was less than 0.5 of the expected value for an electron.

The selection criteria described above made it possible to significantly reduce the hadron background in the elastic events. The main corrections to the experimental data had the same nature as in the earlier experiment at Serpukhov. The geometrical efficiency in this experiment was close to 100% in almost the complete range of q^2 (Fig. 19). Since the search for and reconstruction of elastic events constitute a

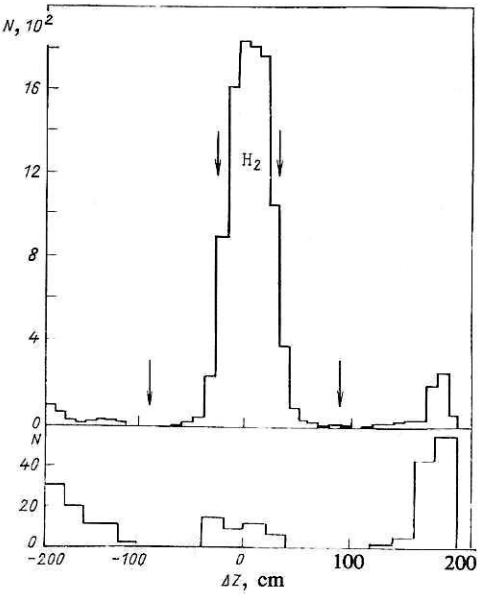

FIG. 17. The top part of the figure shows the Z coordinate of the reconstructed vertex in the target relative to the target center. The arrows indicate the ends of the target flask and the upstream and downstream vertex cuts. At the bottom there is the same distribution obtained during target-empty running. The small number of events in the target region is consistent with scattering on the expected amount of hydrogen vapor in the target volume.

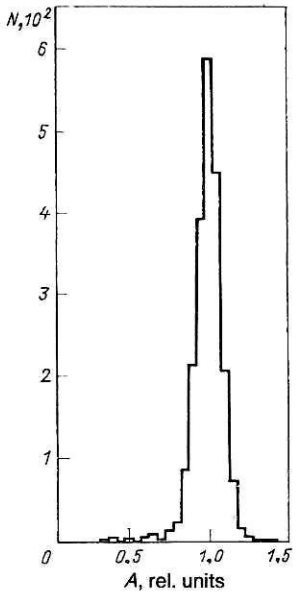

FIG. 18. Distribution of the pulse heights (normalized by the electron energy) from the lead glass shower counters in the experiment at 100 GeV.

difficult problem, much attention was paid to the determination of the efficiency of the event search. To this end, the experimental data were analyzed by two independent programs of geometrical reconstruction of the events. The efficiency of event finding was determined by means of Monte Carlo generated events. As a result, it was found that the inefficiency of the spectrometer and the event-search program was $(0.9 \pm 0.5)\%$. All the corrections used to analyze the experimental data are given in Table IX.

The values obtained for the square of the pion form factor are given in Table X and Fig. 20. The data were approximated by means of a pole expression. The pion charge radius was found to be

$$\langle r_{\pi}^2 \rangle^{1/2} = (0.56 \pm 0.04) \text{ F.}$$

Like the result of the previous experiment, this value agrees with the prediction of the vector-dominance model. To test the sensitivity of the result to the form of the approximation, the data were also approximated by dipole and linear dependences. The results are given in Table XI. It can be seen that the value obtained for the radius is insensitive to the form of the approximation.

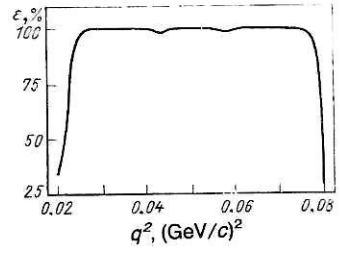

FIG. 19. Geometrical efficiency for elastic πe scattering events in the experiment at 100 GeV.

Elastic πe and Ke Scattering at 250 GeV (Refs. 50, 94, and 99)

Experiments to study the electromagnetic form factors of the pion and kaon in πe and Ke elastic scattering at 250 GeV were proposed in 1975 by the group of physicists doing the πe scattering experiment at 100 GeV. An experimental system was created on the basis of the spectrometer used in the previous experiment, together with a system of high-precision drift chambers prepared at the Joint Institute. The arrangement of the experiment is shown in Fig. 21. A beam of pions and kaons with momentum 250 GeV/c and $\Delta P/P = \pm 0.2\%$ was used. For better geometrical efficiency, the beam was focused on the trigger hodoscope onto a spot measuring about 1 cm^2. This size was determined largely by multiple scattering in the channel. To separate the kaons in the pion beam, a gas-differential Cherenkov counter of length 30 m was used; it was filled with helium at a pressure of about 88.26 kPa (0.9 kgf/cm^2). There were about 2% kaons in the beam. At an intensity of about 10^6 particles/spill, about 20 000 kaons passed through the system. Since it was necessary to improve the spatial and angular resolution of the spectrometer appreciably, drift chambers were included in it to measure the trajectory of the primary particle and the secondary particles after the target, and the spark chambers of the third block of the spectrometer were replaced by proportional chambers.

The spectrometer used four drift-chamber blocks, each of which contained four X planes and four Y planes in one gas space. The external appearance of a module, measuring 25×25 cm, is shown in Fig. 22. The electrical circuit of the chambers was based on the principle of shaping the electric field in the drift chamber by means of wire electrodes. The maximal drift length was 21 mm. To eliminate left–right ambiguity, the pulse wires of neighboring planes were shifted relative to each other by 21 mm. The working gas was a mixture of argon (66.3%), isobutane (30.3%), and methylal vapor (3.4%).

The experiment achieved a record coordinate accuracy for drift chambers. Figure 23 shows the dependence of the coordinate accuracy of the drift chambers on the distance from the pulse wire as determined using data obtained at beam intensity 5×10^4 sec^{-1}. The mean coordinate accuracy is 55 μm. Under the real conditions of the experiment, the coordinate accuracy of the drift chambers was not worse than 100 μm. Because of the use of drift chambers, the angular accuracy of the second block of the spectrometer was 10 μrad.

Because the maximal emission angle of the secondary particles in this experiment was not more than 5 mrad, both particles could enter the same drift gap in the drift chamber placed immediately after the target. Therefore, another important characteristic of the drift chambers was the two-track resolution, i.e., the possibility of detecting two pulses from one wire. Figure 24 shows the efficiency of detection of a second signal as a function of the distance between the first and second tracks. The two-track resolution is basically determined by the width of the pulse from the wire (20–50 nsec), and in the given case was about 2.2 cm.

The use of the drift chambers made it possible to signifi-

TABLE IX. Experimental corrections to the differential cross section in the πe scattering experiment at 100 GeV.

Effect	Correction, %	Error, %
Corrections independent of q^2		
Inefficiency of event search	0,91	0,54
Inefficiency of spectrometer triggering system	0,12	0,45
Density of electrons in the target	0,00	0,27
Presence in the beam of μ^-, e^-, K^-, $\bar{p}$	0,40	0,20
Beam particles outside the total-momentum cuts	2,70	0,12
Absorption of secondary pions	4,71	0,10
Absorption and decay of beam pions	3,06	0,07
δ electrons in the counter A 5	0,39	0,04
Range of variation of the q^2-dependent corrections		
Emission in the target material and the spectrometer	17,4—26,8	0,5
Radiation correction	7,3—8,8	0,4
Strong-interaction background	0,1—0,9	0,4
Admixture of μe events	0,0—0,5	0,2
Correction for geometrical efficiency	0,6—4,7	0,1
Decay of secondary pions	0,4—1,1	0,1

cantly improve the resolution of the spectrometer with respect to the transverse momentum (Fig. 25). The mean imbalance of the transverse momentum for elastic πe scattering events was 8 MeV/c. This imbalance was basically determined by the radiation losses of the secondary electron. It should be noted that these losses hardly cause an imbalance of the coplanarity, where the effect of introducing the drift chambers is therefore manifested more strongly. The introduction of the drift chambers reduced the contribution of the strong-interaction background processes by 5–10 times and made it possible to significantly improve the accuracy in the reconstruction of the event vertex. The coordinate information from the drift chambers (eight coordinates per track) made it possible to reduce to a minimum the reconstruction of spurious tracks. In the investigated πe and Ke scattering reactions at 250 GeV an important condition was the requirement of the detection of closely spaced pairs of secondary particles (about 1 mrad in the X or Y projections). The geometry with displaced wires in the drift chambers made it possible to separate two tracks if the distance between them was more than about 0.3–0.5 mm, which is about an order of magnitude better than in the case of proportional chambers.

To identify the electrons, a system of Cherenkov shower counters was made. It consisted of 12 blocks of lead glass SF 2 and SF 5 measuring $20\times20\times40$ cm and three blocks of glass SF 2 measuring $12.5\times20\times40$ cm. The blocks were arranged in threes along the direction of the beam and horizontally took the form of a five-section hodoscope. Each block was scanned by a photomultiplier from the top. The total length of the three blocks along the beam direction was 20 radiation units. To improve the discrimination between hadrons and electrons, an additional lead radiator of thickness 1 radiation unit was placed in front of the first row of glasses. The counters were calibrated by means of an elec-

TABLE X. Square of the pion form factor measured in the πe scattering experiment at 100 GeV.

Number of point	q^2, (GeV/c)^2	$\lvert F_\pi\rvert^2$	Total error
1	0,0317	0,903	0,026
2	0,0337	0,910	0,027
3	0,0358	0,927	0,030
4	0,0378	0,988	0,033
5	0,0399	0,911	0,034
6	0,0419	0,930	0,038
7	0,0439	0,879	0.039
8	0,0460	0,881	0,040
9	0,0480	0,880	0,043
10	0,0501	0,927	0,047
11	0,0521	0,971	0,052
12	0,0542	0,915	0,054
13	0,0562	0,735	0,053
14	0,0583	0,779	0,059
15	0,0603	0,853	0,065
16	0,0623	0,870	0,071
17	0,0644	0,818	0,075
18	0,0664	0,813	0,081
19	0,0685	0,790	0,087
20	0,0705	0,768	0,095

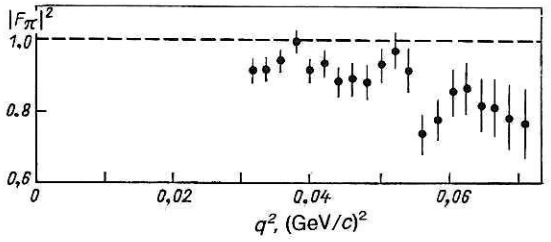

FIG. 20. Square of the pion form factor in the experiment at 100 GeV.

tron beam with energy 35, 70, and 97 GeV. It was found that, as a percentage, the energy resolution can be well described by the expression

$$\sigma = \pm 15/\sqrt{E},$$

where E (GeV) is the electron energy. To form the trigger pulse, the counters were combined into four groups, each of two neighboring sections. If the pulse from some group of counters exceeded the discrimination level, this indicated the passage of a particle that had lost an appreciable fraction of its energy on producing a shower.

The logic for selecting beam particles and the system trigger were basically organized as in the previous πe scattering experiment at 100 GeV. An interesting feature of the experiment was the automatic regime for triggering the system from the beam monitor during the collection of statistics in order to maintain a continuous check on the beam parameters. The system was triggered by both Ke and πe events. Only every fourth pion passing through the system was examined as a candidate for πe triggering. The triggering system contained two electronic logic circuits for each type of triggering.

The electromagnetic radius of the K^- meson was measured in this experiment for the first time. About 2000 elastic Ke scattering events were recorded. The procedure already described above for the identification and kinematic analysis of events was used in the selection of the events. The quality of the geometrical reconstruction is illustrated by the distribution of the reconstructed Z coordinate of the interaction vertex in the target (Fig. 26).The location and length of the target are well reproduced. The additional peaks correspond to kaon scattering by the vacuum windows of the target and the proportional chambers situated near the ends of the target.

The χ^2 distribution of the events is shown in Fig. 27. The tail of the distribution is to a large degree due to elastic scattering events in which the secondary kaon decayed or underwent nuclear scattering in the target or spectrometer. The energy distribution is shown in Fig. 28. The distribution of the pulse heights (normalized by the electron energy) from the Cherenkov shower counters is shown in Fig. 29. The tail of the distribution at large pulse heights is due to kaons that entered the same lead glass block as the electron. The selected events had to have Z coordinate of the interaction vertex within 84 cm of the center of the target, χ^2 less than 30, photon energy less than 12 GeV, and normalized pulse height greater than 0.8.

The experimental corrections to the data used to determine the Ke differential cross section are given in Table XII.

The values of the square of the kaon form factor are given in Table XIII. The data were approximated by means of a pole expression (Fig. 30). The charge radius of the K^- meson was found to be

$$\langle r_K^2 \rangle^{1/2} = (0.53 \pm 0.05) \quad \text{F}.$$

The error in this result is determined largely by the statistics. The values of the square of the form factor obtained as a result of the approximation are shown by the continuous curve in Fig. 30. For approximation of the form factor without normalization (broken curve), the kaon radius is found to be 0.65 ± 0.15 F, and $|F_\pi|^2 = 1.07 \pm 0.09$ at $q^2 = 0$. This indicates internal consistency of the result. Use of a dipole approximation gives a slight difference in the kaon radius. When the systematic uncertainty in the data is tripled, the kaon radius is found to be 0.54 ± 0.07 F. Thus, the result is insensitive to systematic error in the data. The kaon radius 0.53 ± 0.05 F obtained in the experiment agrees well with the predictions of the Chou–Yang geometrical model of hadron scattering[69]: 0.54 ± 0.14 F, the model of relativistic quark diagrams (0.53 F),[75] the parton model (0.52 F),[77] and the vector-dominance model (0.58 F).

Gerasimov[100] and Greenberg *et al.*[101] derived in the nonrelativistic quark model an inequality relating the ratio of the masses of the strange (m_s) and ordinary (m_u) quarks to the ratio of the electromagnetic radii of the neutral and charged kaons.

$$r^2(K^0)/r^2(K^-) = -(m_s^2 - m_u^2)/(2m_s^2 + m_u^2).$$

TABLE XI. Value of $\langle r_\pi^2 \rangle$ obtained using different forms of approximation.

Form of approximation	$\lvert F_\pi(q^2)\rvert^2$	$\langle r_\pi^2 \rangle$, F^2
Pole	$\left(1+\frac{1}{6}\langle r_\pi^2\rangle q^2\right)^{-2}$	0.31±0.04
Dipole	$\left(1+\frac{1}{12}\langle r_\pi^2\rangle q^2\right)^{-4}$	0.31±0.04
Linear	$\left(1-\frac{1}{6}\langle r_\pi^2\rangle q^2\right)^{-2}$	0.30±0.04

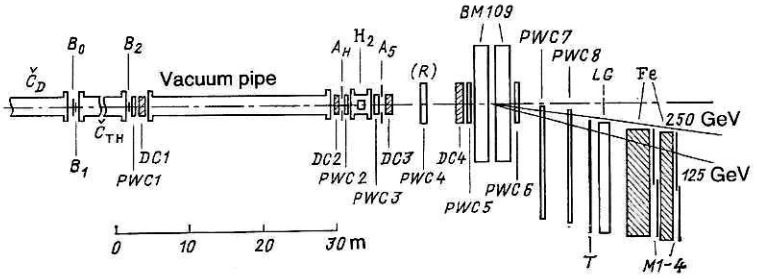

FIG. 21. Arrangement of the πe and Ke scattering experiments at 250 GeV. B_0, B_1, B_2 are monitor scintillation counters, $\check{C}_D$ is a differential Cherenkov counter, *PWC* 1–8 are proportional chambers, *DC* 1–4 are drift chambers, (*R*) are rotated chambers, A_H and A 5 are anticoincidence scintillation counters, H_2 is a liquid-hydrogen target, *BM* 109 are analyzing magnets, *T* is a rigger hodoscope, Fe is an iron absorber, *M* 1–4 are muon scintillation counters, and *LG* is a lead glass Cherenkov spectrometer.

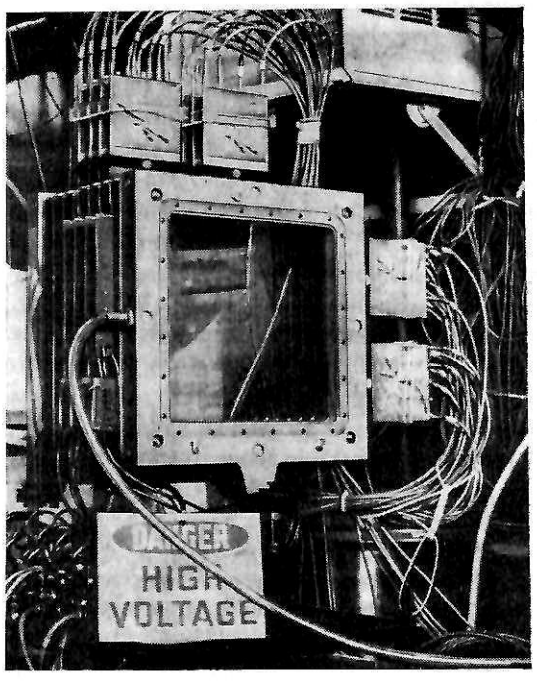

FIG. 22. External appearance of a module of drift chambers with working region measuring 25×25 cm.

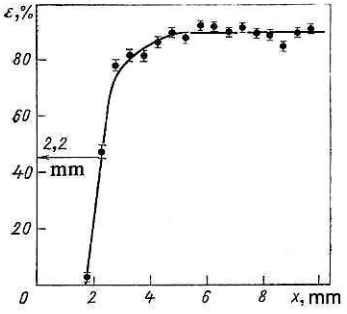

FIG. 24. Dependence of the efficiency of detection of a second pulse in a drift chamber on the distance between the tracks.

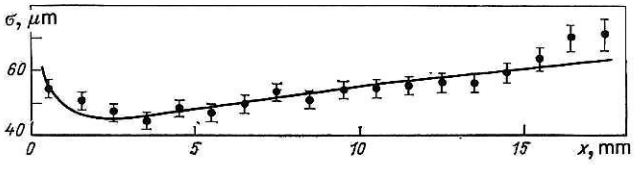

FIG. 23. Dependence of the coordinate accuracy of a drift chamber on the distance from the pulse wire, obtained in the experiment at 250 GeV. The mean coordinate accuracy is 55 μm.

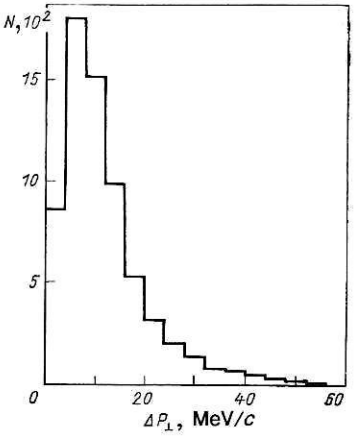

FIG. 25. Imbalance of the transverse momentum for elastic πe scattering events in the experiment at 250 GeV.

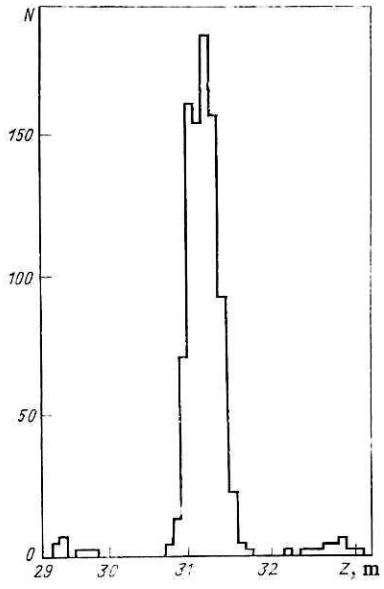

FIG. 26 Distribution of the Z coordinate of the reconstructed vertex for Ke scattering events.

The electromagnetic radius of the neutral kaon has been measured in a kaon regeneration experiment[102]:

$$\langle r^2_{K^0} \rangle = -(0.054 \pm 0.026) \text{ F}^2.$$

Taking the ratio of the radii of the neutral and charged kaons, we obtain for the quark masses

$$m_s/m_u \geqslant 1.39 \pm 0.28.$$

In the experiment at 250 GeV, about 15 000 elastic πe scattering events were also detected. The results on the pion form factor are given in Table XIV and in Fig. 31. The data were approximated by a pole expression (continuous curve). The value obtained for the pion radius was

$$\langle r^2_{\pi} \rangle^{1/2} = (0{,}66 \pm 0.03) \text{ F}.$$

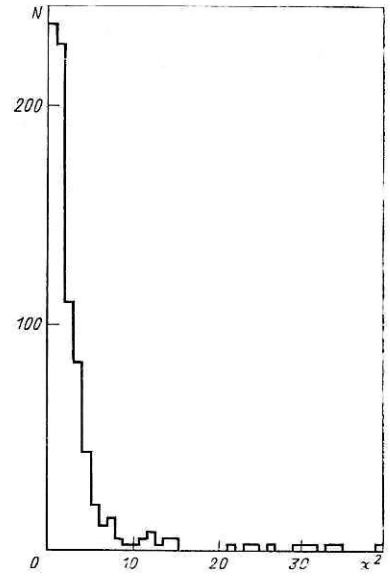

FIG. 27. The χ^2 distribution for the selected Ke scattering events.

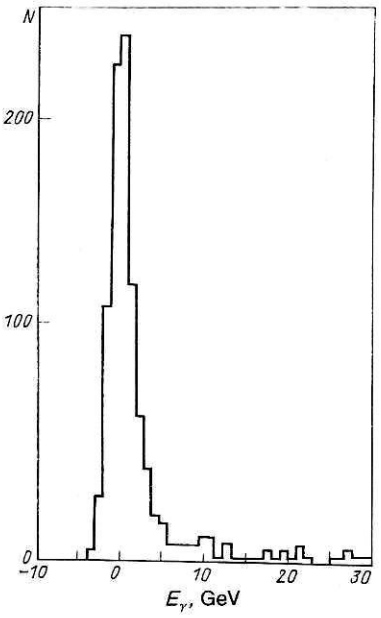

FIG. 28. Distribution of the photon energy, obtained by kinematic analysis of the Ke scattering events.

When the data were approximated without normalization (broken curve), the results was $\langle r^2_{\pi} \rangle^{1/2} = 0.62 \pm 0.09$ F and $|F_{\pi}|^2 = 0.974 \pm 0.039$ at $q^2 = 0$.

The data obtained in the three elastic πe scattering experiments were approximated simultaneously and in different combinations (Table XV). The simultaneous approximation of the data of all three experiments (Fig. 32) gives the pion radius.

$$\langle r^2_{\pi} \rangle^{1/2} = (0.636 \pm 0.024) \text{ F}.$$

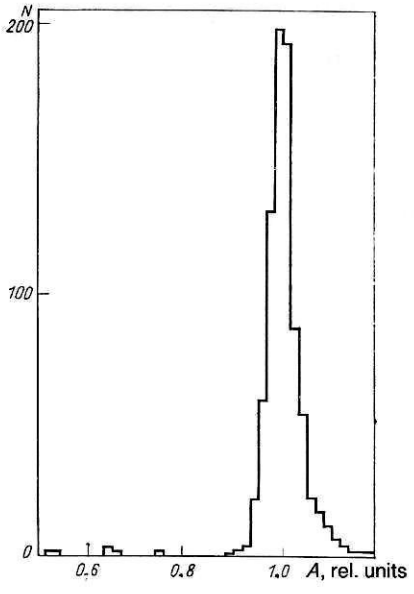

FIG. 29. Distribution of the pulse heights (normalized by the electron energy) from the Cherenkov shower counters for elastic Ke scattering events.

TABLE XII. Experimental corrections to the differential cross section in the Ke scattering experiment at 250 GeV.

Effect	Correction, %	Error, %
Corrections not dependent on q^2		
Beam particles outside the total-momentum cuts	0.5	0.1
Presence of e, μ, π, and $\bar{p}$ in the beam	0.1	0.2
Decays of beam kaons	1.5	0.1
Absorption of beam kaons	2.9	0.1
Density of electrons in the target	0.0	0.3
Absorption of secondary kaons	4.1	0.1
Detection of δ electrons in the counter A5	0.4	0.1
Trigger inefficiency	0.2	0.2
Range of variation of the q^2-dependent corrections		
Geometical inefficiency	0.0 – 13.1	0.0 – 0.4
Radiation correction	4.1 – 10.5	0.2 – 0.3
Decays of secondary kaons	1.4 – 2.1	0.1 – 0.1
Hadron background	0.0 – 1.7	0.0 – 1.2
Inefficiency of event search	2.7 – 4.0	0.5 – 0.6
Emission in the target material and the spectrometer	13.9 – 25.6	0.2 – 0.3

with χ^2 equal to 51.0 for 55 degrees of freedom. The value of the square of the form factor obtained as a result of the approximation is shown by the continuous curve in Fig. 32. For approximation of the data without normalization (broken curve) $\langle r_\pi^2 \rangle^{1/2} = 0.67 \pm 0.07$ F and $|F_\pi|^2 = 1.021 \pm 0.027$ at $q^2 = 0$.

Table XV gives the value of χ^2 for approximation of the data in different combinations and separately. It can be seen that the data of the three experiments are well approximated simultaneously. However, the individual results of the experiments indicate a possible presence of some systematic errors in the data. Thus, the square of the pion radius obtained in the E100 experiment is 2.1 standard deviations smaller than the result obtained in the case of the simultaneous approximation, while the square of the pion radius from the experiments E50 and E250 is, respectively, 1.4 and 1.2 standard deviations larger. These discrepancies suggest that the errors of the combined result of the three experiments should be calculated using a factor of the form $(\Sigma\sigma_i^2/(n-1))^{1/2}$, where σ_i is the normalized deviation of the result of each experiment from the mean value and $n = 3$ is the number of experiments. [This is the method used by the Particle Data Group.]

Correcting the error in this way, Dally *et al.*[50] obtained for the pion radius with the simultaneous approximation of the three experiments the value

$$\langle r_\pi^2 \rangle^{1/2} = (0.636 \pm 0.037) \text{ F}.$$

As can be seen from Table IV, this result agrees with many theoretical predictions for the charge radius of the pion. In Ref. 72, an attempt was made to approximate the pion form factor simultaneously in the spacelike and timelike regions of momentum transfers $(-9.77 < q^2 < 9.61$ $(\text{GeV}/c)^2)$ by a method that depends weakly on theoretical models. The pion radius was found to be 0.69 ± 0.02 F. This result differs somewhat from the combined result of the πe scattering experiments. However, if from the set of data the data from the pion electroproduction experiments[22] are removed, the pion radius is found to be 0.66 ± 0.02 F, which agrees well both with the result of the last πe scattering experiment and with the combined result of the three experiments.

The simultaneous measurement of the elastic scattering of pions and kaons by electrons at 250 GeV makes possible a direct experimental comparison of their form factors[103] in the region of momentum transfers $0.037 \leqslant q^2 \leqslant 0.094$ $(\text{GeV}/c)^2$. Such a comparison makes it possible to eliminate possible ignored systematic errors that could be present in the individual results. In this experiment, the conditions for detection of the πe and Ke scattering events were almost identical. The same selection criteria were used to analyze the data on both types of event. The main corrections to the differen-

TABLE XIII. Square of the kaon form factor measured in the Ke scattering experiment at 250 GeV.

Number of point	q^2, $(\text{GeV}/c)^2$	$\lvert F_K \rvert^2$	Total error
1	0.0409	0.93	0.03
2	0.0491	0.90	0.04
3	0.0572	0.89	0.05
4	0.0654	0.85	0.06
5	0.0736	0.79	0.07
6	0.0818	0.90	0.09
7	0.0899	0.67	0.10
8	0.0981	0.77	0.13
9	0.1063	0.76	0.16
10	0.1145	0.90	0.23

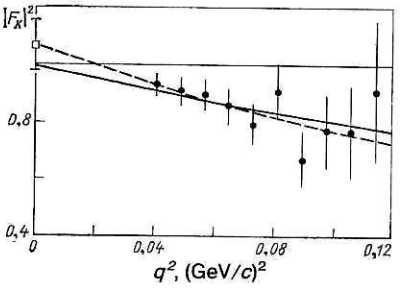

FIG. 30. Square of the form factor of the K^- meson.

TABLE XIV. Square of the pion form factor measured in the πe scattering experiment at 250 GeV.

Number of point	q^2 (GeV/c)^2	$\lvert F_\pi \rvert^2$	Total error
1	0.0388	0.857	0.019
2	0.0429	0.865	0.021
3	0.0470	0.821	0.022
4	0.0511	0.840	0.024
5	0.0522	0.831	0.025
6	0.0593	0.767	0.027
7	0.0634	0.838	0.029
8	0.0675	0.757	0.032
9	0.0715	0.791	0.035
10	0.0756	0.762	0.038
11	0.0797	0.765	0.041
12	0.0838	0.802	0.045
13	0.0879	0.720	0.047
14	0.0920	0.728	0.050

tial cross sections, such as allowance for the absorption of the primary particles, radiation by the electrons, the efficiency of the event search, the radiation correction, and the triggering inefficiency, differed little for the two types of event and largely compensated each other as regards the form factors. According to the estimates of the authors, the total systematic uncertainty in the ratio of the cross sections could not have exceeded 1%.

The ratio of the squares of the kaon and pion form factors, shown in Fig. 33, was approximated by an expression of the form

$$\frac{|F_K|^2}{|F_\pi|^2} = 1 + q^2 (\langle r_\pi^2 \rangle - \langle r_K^2 \rangle) [1 + q^2 (\langle r_\pi^2 \rangle - 3 \langle r_K^2 \rangle)/12]/3.$$

The $(\langle R_\pi^2 \rangle - 3\langle r_K^2 \rangle)$ term, which gives a small contribution, was determined with allowance for the data obtained in the experiment at 250 GeV for the pion radius, $\langle r_\pi^2 \rangle = 0.439$ F^2, and the kaon radius, $\langle r_K^2 \rangle = 0.28$ F^2. As a result, it was found that

$$\langle r_\pi^2 \rangle - \langle r_K^2 \rangle = (0.16 \pm 0.06) \text{ F}^2$$

with $\chi^2 = 3.5$ for six degrees of freedom.

One can compare the experimentally measured kaon radius with the value obtained from the difference of the squares of the pion and kaon radii. If the square of the pion radius $\langle r_\pi^2 \rangle = 0.47 \pm 0.02$ F^2 is taken from Ref. 72, in which the pion form factor was approximated in the region of q^2 from -9.77 to 9.66 (GeV/c)^2, then $\langle r_K^2 \rangle = 0.31 \pm 0.06$ F^2.

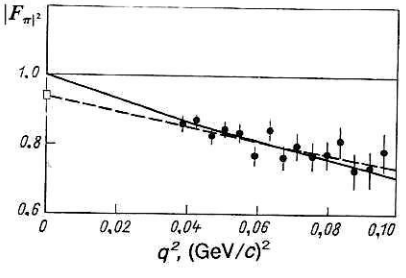

FIG. 31. Square of the pion form factor measured in the experiment at 250 GeV.

Taking for the square of the pion radius the value $\langle r_\pi^2 \rangle = 0.43$ F^2 obtained by approximation of the experimental data[72] without allowance for the electroproduction experiments, we obtain $\langle r_K^2 \rangle = 0.27 \pm 0.06$ F^2. But if we use the combined result of the three πe elastic-scattering experiments ($\langle r_\pi^2 \rangle = 0.405$ F^2), then the kaon charge radius will be 0.24 ± 0.06 F. It can be seen that in all cases good agreement with the experimentally measured kaon radius [$\langle r_K^2 \rangle = 0.28 \pm 0.05$ F^2] is observed.

According to the vector-dominance model, the ratio of the difference of the squares of the radii of the charged pion and charged kaon to the square of the radius of the neutral kaon satisfies

$$R = \frac{\langle r_{\pi^-}^2 \rangle - \langle r_{K^-}^2 \rangle}{\langle r_{K^0}^2 \rangle} = -1.0.$$

If we take into account the value for the radius of the neutral kaon,[102] then

$$R = -3.0 \pm 1.8,$$

which is in some disagreement with the vector-dominance model. However, it was shown in Ref. 104 that when allowance is made in this model for the breaking of $SU(3)$ associated with the mass difference of the quarks $R = -2.5$, which agrees better with the experimental results.

Elastic πe and Ke Scattering at 300 GeV (Ref. 51)

An experiment to investigate the electromagnetic form factors of the pion and kaon in elastic πe and Ke scattering experiments at 300 GeV was proposed in 1977 at CERN (experiment HA-7). In this experiment, it was proposed to make measurements in the region of momentum transfers up to 0.29 (GeV/c)^2 for πe scattering and up to 0.17 (GeV/c)^2 for Ke scattering. To a considerable degree, the experiment took into account the experience gained from the similar experiments at Serpukhov and Batavia.

The experiment was based on the spectrometer FRAMM.[105] This spectrometer consists of four analyzing magnets arranged successively along the direction of the beam. The particle trajectories are detected by means of a

TABLE XV. Results of approximation of the data of three experiments on πe scattering at energies 50 (E 50), 100 (E 100), and 250 (E 250) GeV.

Experiment	Number of points	$\lvert F_\pi \rvert^2_{q^2=0} = 1$		$\lvert F_\pi \rvert^2_{q^2=0}$ = free parameter		
		$\langle r^2_\pi \rangle$	χ^2	$\langle r^2_\pi \rangle$	Normalization	χ^2
$E50 + E100 + E250$	56	0,405±0,024	51,0	0,454±0,067	1,021±0,027	50,3
$E50 + E100$	42	0,339±0,040	37,2	0,420±0,118	1,029±0,040	36,6
$E50 + E250$	36	0,447±0,029	20,8	0,421±0,076	0,988±0,032	20,6
$E100 + E250$	34	0,399±0,024	39,2	0,453±0,073	1,024±0,030	38,5
$E50$	22	0,610±0,150	9,6	1,024±0,348	1,106±0,080	7,7
$E100$	20	0,315±0,041	23,5	0,418±0,145	1,039±0,052	22,9
$E250$	14	0,439±0,030	9,8	0,384±0,088	0,974±0,039	9,3

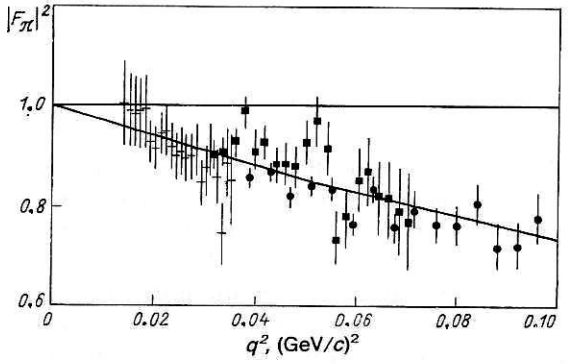

FIG. 32. Square of the pion form factor obtained in the elastic πe scattering experiments: Serpukhov, 50 GeV (crosses); Batavia, 100 GeV (black squares); Batavia, 250 GeV (black circles).

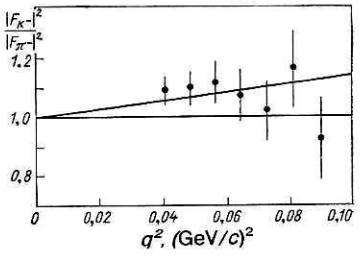

FIG. 33. Ratio of the squares of the kaon and pion form factors obtained in the 250-GeV experiment.

system of drift chambers placed between the magnets. In front of the magnets there are scintillation counters and electron detectors to detect the secondary electrons deflected in each magnet. The momentum resolution of the spectrometer is $\pm$ 0.5% and does not depend on the particle momentum.

For the πe and Ke scattering experiment proportional chambers, a liquid-hydrogen target, and scintillation counters were placed in front of the spectrometer (Fig. 34). The trajectories of the primary particle and the secondary particles were detected by proportional chambers. Pulses from the scintillation counters and the detectors used to identify the electrons serve to trigger the system.

According to the preliminary data obtained in this experiment,[106] the rms pion radius is

$$\langle r^2_\pi \rangle^{1/2} = (0{,}68 \pm 0{,}09)\ \text{F}.$$

CONCLUSIONS

Considerable progress has been achieved in recent years in investigations of the electromagnetic sizes of the pion and kaon.

A further improvement in the accuracy of the experimental results requires an increase in the beam energy and progress in the experimental techniques.

The commissioning in the foreseeable future of accelerators with beam energy of secondary particles up to 1 TeV and more will make it possible not only to significantly im-

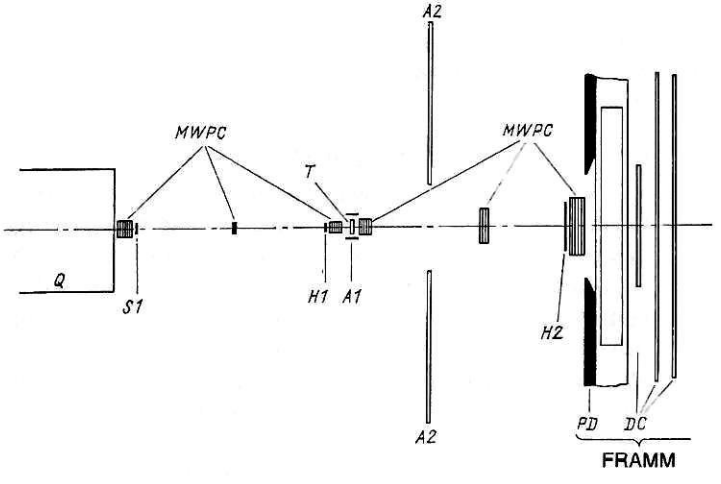

FIG. 34. Arrangement of the experiment for investigating elastic πe and Ke scattering at 300 GeV at CERN: Q is a quadrupole lens, $MWPC$ are proportional chambers, T is a liquid-hydrogen target, H 1 and H 2 are scintillation hodoscopes, A 1 and A 2 are anticoincidence scintillation counters, PD is an electron detector, DC are drift chambers, and S 1 is a scintillation counter.

prove the accuracy in the measurement of the pion and kaon radii but also to make direct measurements of the shape of their charge distribution. Secondary beams of hyperons with energies of a few hundred GeV will make it possible to begin the investigation of the electromagnetic sizes of the charged hyperons.

The successes now achieved in quantum chromodynamics open up a prospect of predictions in the near future of the detailed shape of the charge distribution in hadrons. Then experiments in which unstable hadrons are scattered by electrons will be a source of valuable information about the dynamical structure of bound states of quarks and will contribute to solving the problem of their confinement.

[1]R. Hofstadter and R. W. McAllister, Phys. Rev. **98** 217 (1955).
[2]Y. Nambu, Phys. Rev. **106**, 1366 (1957).
[3]W. R. Frazer and J. R. Fulco, Phys. Rev. Lett. **2**, 365 (1959).
[4]J. J. Sakurai, Ann. Phys. (N.Y.) **11**, 1 (1960).
[5]H. Frauenfelder and E. M. Henley, Subatomic Physics, Prentice-Hall, Englewood Cliffs, N. J. (1974) [Russian translation published by Mir, Moscow (1979)].
[6]N. F. Mott, Proc. R. Soc. London Ser. A **124**, 425 (1929).
[7]E. Guth, Anz. Akad. Wiss. Wien **71**, 299 (1934).
[8]M. E. Rose, Phys. Rev. **73**, 279 (1948).
[9]S. D. Drell and F. Zachariasen, Electromagnetic Structure of Nucleons, Oxford University Press, London (1961) [Russian translation published by Izd. Inostr. Lit., Moscow (1962)].
[10]R. R. Wilson, Phys. Today **1**, 47 (1969).
[11]M. Gourdin, Phys. Rep. **11**, 29 (1974).
[12]M. Nordberg, Jr. and K. Kinsey, Phys. Lett. **20**, 692 (1966).
[13]M. M. Block, I. Kenyon, J. Keren, *et al.*, Phys. Rev. **160**, 1074 (1968).
[14]K. M. Crowe, A. Fainberg, J. Miller, and A. S. L. Parsons, Phys. Rev. **180**, 1349 (1969).
[15]R. A. Christensen, Phys. Rev. D **1**, 1469 (1970)
[16]F. Nichitiu and Yu. A. Shcherbakov, Nucl. Phys. **B61**, 429 (1973).
[17]E. H. Auerbach, D. M. Fleming, and M. M. Sternheim, Phys. Rev. **162**, 1683 (1967).
[18]L. Aleksandrov, T. Angelescu, F. Nichitiu, *et al.*, Soobshchenie (Communication) R1-8328, JINR, Dubna (1974).
[19]C. W. Akerlof, W. W. Ash, K. Berkelman, *et al.*, Phys. Rev. **163**, 1482 (1967).
[20]C. Mistretta, D. Imric, J. A. Appel, *et al.*, Phys. Rev. Lett. **20**, 1523 (1968).
[21]C. J. Bebek, C. N. Brown, M. Herzlinger, *et al.*, Phys. Rev. D **13**, 25 (1976).
[22]C. J. Bebek, C. N. Brown, S. D. Holmes, *et al.*, Phys. Rev. D **17**, 1693 (1978).
[23]C. Bardin, J. Duclos, A. Magnon, *et al.*, Nucl. Phys. **B120**, 45 (1977).
[24]W. R. Frazer, Phys. Rev. **115**, 1763 (1959).
[25]F. A. Berends, Phys. Rev. D **1**, 2590 (1970).
[26]B. H. Kellet and C. Verzegnassi, Nuovo Cimento **A13**, 195 (1973).
[27]N. Dombey and B. J. Read, Nucl. Phys. **B60**, 65 (1973).
[28]S. Devons, D. Nemethy, C. Nissim-Sabat, *et al.*, Phys. Rev. **184**, 1345 (1969).
[29]S. F. Berezhnev, T. D. Blokhintseva, A. V. Dem'yanov, *et al.*, Yad. Fiz. **26**, 547 (1977) [Sov. J. Nucl. Phys. **26**, 290 (1977)].
[30]S. F. Berezhnev, T. D. Blokhintseva, A. V. Dem'yanov, *et al.*, Preprint R1-9575 [in Russian], JINR, Dubna (1976).
[31]T. D. Blokhintseva, Yu. A. Surovtsev, and F. G. Tkebuchava, Yad. Fiz. **21**, 850 (1975) [Sov. J. Nucl. Phys. **21**, 438 (1975)].
[32]N. M. Budnev, V. M. Budnev, and V. V. Serebryakov, Phys. Lett. **B64**, 307 (1976).
[33]G. Hohler and E. Pietarinen, Nucl. Phys. **B95**, 210 (1975).
[34]J. E. Augustin, J. C. Bizot, J.Buon, *et al.*, Phys. Rev. Lett. **20**, 126 (1968).
[35]V. L. Auslender, G. I. Budker, Yu. N. Pestov, *et al.*, Phys. Lett. **B25**, 433 (1967).
[36]D. Benaksas, G. Cosme, B. Jean-Marie, *et al.*, Phys. Lett. **B39**, 289 (1972).
[37]A. Quenzer, M. Ribes, F. Rumpf, *et al.*, Phys. Lett. **B76**, 512 (1978)
[38]I. B. Vasserman, P. M. Ivanov, G. Ya. Kezerashvili, *et al.*, Preprint 80-169 [in Russian], Institute of Nuclear Physics, Siberian Division, USSR Academy of Sciences, Novosibirsk (1980).
[39]A. Minten, Preprint CERN 69-22, Geneva (1969).
[40]G. Gounaris and J. J. Sakurai, Phys. Rev. Lett. **21**, 244 (1968).
[41]N. M. Budnev, V. M. Budnev, and V. V. Serebryakov, Phys. Lett. **B64**, 307 (1976)
[42]A. Costa de Beauregard, T. N. Pham, B. Pire, and T. N. Truong, Phys. Lett. **B67**, 213 (1977).
[43]F. S. Crawford, Jr., Phys. Rev. **117**, 1119 (1960).
[44]V. G. Grishin, E. P. Kistenev, and Mu Tszyun', Yad. Fiz. **2**, 836 (1965) [Sov. J. Nucl. Phys. **2**, 589 (1966)].
[45]J. Allan, G. Ekspong, and P. Sallstrom, Nuovo Cimento **32**, 1144 (1964).
[46]J. Samini, R. L. Kinzer, and J. R. Burwell, Phys. Rev. D **17**, 1979 (1979).
[47]D. G. Cassel, Experimental Measurement of the Electromagnetic Form Factor of the Negative π-Meson, Ph.D. Thesis, Princeton University (1965).
[48]G. T. Adylov, F. K. Aliev, D. Yu. Bardin, *et al.*, Nucl. Phys. **B128**, 461 (1977).
[49]E. B. Dally, D. J. Drickey, J. M. Hauptman, *et al.*, Phys. Rev. D **24**, 1718 (1981).
[50]E. B. Dally, J. M. Hauptman, J. Kubic, *et al.*, Phys. Rev. Lett. **48**, 375 (1982).
[51]G. Bologna, B. D'Ettore Piazzoli, F. L. Fabbri, *et al.*, Preprint CERN/SPSC/1 73–48, CERN, Geneva (1973).
[52]H. I. Bhabha, Proc. R. Soc. London Ser. A **164**, 269 (1938).
[53]H. Salecker, Z. Naturforsch. Teil A **15**, 1023 (1960).
[54]C. F. Cho and J. J. Sakurai, Lett. Nuovo Cimento **2**, 7 (1971).
[55]C. L. Hammer, V. S. Zidell, R. W. Reimer, and T. A. Weber, Phys. Rev. D **15**, 696 (1977).
[56]G. Bonneau and F. Martin, Nucl. Phys. **B97**, 269 (1975).
[57]F. Felicetti and Y. Srivastava, Phys. Lett. **B83**, 109 (1979).
[58]B. V. Geshkenbeĭn, Yad. Fiz. **9**, 1232 (1969) [Sov. J. Nucl. Phys. **9**, 720 (1969)].
[59]X. Y. Pham and A. C. D. Wright, Phys. Rev. D **11**, 1806 (1975).
[60]I. Rasziller and W. Schmidt, Nucl. Phys. **B55**, 106 (1973).
[61]H. D. Kiehlmann and W. Schmidt, Nucl. Phys. **B94**, 67 (1975).
[62]G. Hohler and E. Pietarinen, Phys. Lett. **B53**, 471 (1975).
[63]M. Roos, Preprint, Univ. of Helsinki (1973).
[64]B. B. Deo and M. K. Parida, Phys. Rev. D **13**, 1927 (1976).
[65]S. Dubnicka and V. A. Meshcheryakov, Preprint E2-7982 [in English], JINR, Dubna (1974).
[66]P. M. Gensini, Phys. Rev. D **17**, 1368 (1978).
[67]V. A. Baluni, Phys. Lett. **B38**, 535 (1972).
[68]N. Zovko, Phys. Lett. **B51**, 54 (1975).
[69]T. T. Chou, Phys. Rev. D **19**, 3327 (1979).
[70]M. K. Volkov and V. N. Pervushin, Preprint E2-7283 [in English], JINR, Dubna (1973).
[71]R. Tarrach, Z. Phys. **C2**, 221 (1979).
[72]M. F. Heyn and C. B. Lang, Z.Phys. **C7**, 169 (1981).
[73]N. M. Kroll, T. D. Lee, and B. Zumino, Phys. Rev. **157**, 1376 (1967).
[74]S. Blatnik, J. Stanov, and C. B. Lang, Lett. Nuovo Cimento **24**, 39 (1979).
[75]S. B. Gerasimov, Yad. Fiz. **29**, 513 (1979) [Sov. J. Nucl. Phys. **29**, 259 (1979)].
[76]M. K. Volkov, V. B. Matafonov, and V. N. Pervushin, Preprint R2-8659 [in Russian], JINR, Dubna (1975).
[77]N. Yu. Volkonskiĭ, Yad. Fiz. **30**, 510 (1979) [Sov. J. Nucl. Phys. **30**, 264 (1979)].
[78]F. Felicetti and Y. Srivastava, Phys. Lett. **B107**, 227 (1981).
[79]C. J. Bebek, C. N. Brown, M. Herzlinger, *et al.*, Phys. Rev. Lett. **32**, 21 (1974).
[80]J. C. Bizot, J. Buon, Y. Chatelus, *et al.*, Phys. Lett. **B32**, 416 (1970).
[81]M. Bernardini, D. Bollini, P. L. Brunini, *et al.*, Phys. Lett. **B44**, 393 (1973).
[82]M. Bernardini, D. Bollini, P.L.Brunini, *et al.*, Phys. Lett. **B46**, 261 (1973).
[83]V. E. Balakin, G. I. Budker, E. V. Pakhtusova, *et al.*, Phys. Lett. **B34**, 328 (1971).
[84]V. E. Balakin, G. I. Budker, L. M. Kurdadze, *et al.*, Phys. Lett. **B41**, 205 (1972).
[85]V. A. Sidorov, in: Proc. of the Intern. Conf. on High Energy Physics, Tbilisi (1976), p. B13.
[86]B. Esposito, F. Felicetti, A. Marini, *et al.*, Phys. Lett. **B67**, 239 (1977).
[87]J. C. Bizot, J. Buon, A. Cordier, *et al.*, in. Proc. of the Intern. Conf. on High Energy Physics, Geneva (1979), p. 362; B. Delcourt, D. Bisello, T. C. Bizot, *et al.*, Phys. Lett. **B99**, 257 (1981).

[88]P. M. Ivanov, L. M. Kurdadze, M. Yu. Lelchuk *et al.*, Preprint INP 79-68, Novosibirsk (1979).
[89]B. Esposito, A. Marini, G. Piano-Montari, *et al.*, Lett. Nuovo Cimento **28**, 337 (1980).
[90]V. A. Sidorov, in: Proc. of the Intern. Photon Conf. at High Energies, Batavia (1979), p. 490.
[91]P. M. Ivanov, L. M. Kurdadze, M. Yu. Lelchuk, *et al.*, Phys. Lett. **B107**, 297 (1981).
[92]N. M. Budnev, V. M. Budnev, and V. V. Serebryakov, Phys. Lett. **B70**, 365 (1977).
[93]V. I. Baĭer and V. S. Fadin, Pis'ma Zh. Eksp. Teor. Fiz. **15**, 219 (1972) [JETP Lett. **15**, 151 (1972)].
[94]E. B. Dally, J. M. Hauptman, J. Kubic, *et al.*, Phys. Rev. Lett. **45**, 232 (1980); A. Beretvas, E. Dally, Z. Guzik, *et al.*, Preprint E1-12357 [in-English], JINR, Dubna (1979).
[95]D. Yu. Bardin, O. Czyyzewski, T. Dobrowolski, *et al.*, Preprint E1-4786 [in English], JINR, Dubna (1969).
[96]L. B. Golovanov, Fiz. Elem. Chastits At. Yadra **2**, No. 3, 717 (1972) [Sov. J. Part. Nucl. **2**, 126 (1972)].
[97]D. Yu. Bardin, G. V. Micelmacher, and N. M. Shumeiko, Preprint E2-6235 [in English], JINR, Dubna (1972).
[98]J. Hauptman, D. Stork, and A. Watson, Preprint UCLA HEE-044, Los Angeles (1975).
[99]A. S.Vodop'yanov, Dissertatsiya (Dissertation), JINR, Dubna (1981).
[100]S. B. Gerasimov, Zh. Eksp. Teor. Fiz. **50**, 1559 (1966) [Sov. Phys. JETP **23**, 1040 (1966)].
[101]O. W. Greenberg, S. Nussinov, and J. Sucher, Phys. Lett. **B70**, 465 (1977).
[102]W. R. Molzon, J. Hoffnagle, J. Roehrig, *et al.*, Phys. Rev. Lett. **41**, 1213 (1978).
[103]E. B. Dally, J. M. Hauptman, J. Kubic, *et al.*, Contributed paper at the Intern. Conf. on High Energy Physics, Madison (1980); N. Chertok, in: Proc. of the Intern. Conf. on High Energy Physics, Madison (1980), p. 547.
[104]Ll. Ametller, C. Ayala, and A. Bramon, Phys. Rev. D **24**, 233 (1981).
[105]Experiments at CERN in 1981, CERN, Geneva (1981).
[106]H. Shopper, Preprint CERN 81-17, Geneva (1981).

Translated by Julian B. Barbour